Journal of Autoimmunity 148 (2024) 103292

Contents lists available at ScienceDirect

Journal of Autoimmunity

journal homepage: www.elsevier.com/locate/jautimm

Perivascular B cells link intestinal angiogenesis to immunity and to the gut-brain axis during neuroinflammation

Benjamin Peter [a], Jessica Rebeaud [a], Solenne Vigne [a], Valentine Bressoud [a], Nicholas Phillips [a], Florian Ruiz [a], Tatiana V. Petrova [b], Jeremiah Bernier-Latmani [b], Caroline Pot [a,*]

[a] Laboratories of Neuroimmunology, Service of Neurology and Neuroscience Research Center, Department of Clinical Neurosciences, Lausanne University Hospital and University of Lausanne, Epalinges, 1066, Switzerland
[b] Department of Oncology, University of Lausanne and Ludwig Institute for Cancer Research, Epalinges, 1066, Switzerland

ARTICLE INFO

Handling editor: C Selmi

Keywords:
Gut-brain axis
Gut–vascular barrier
Neuroinflammation
Experimental autoimmune encephalomyelitis
Angiogenesis
B cell

ABSTRACT

Disruption of gut barrier function and intestinal immune cell homeostasis are increasingly considered critical players in pathogenesis of extra-intestinal inflammatory diseases, including multiple sclerosis (MS) and its prototypical animal model, the experimental autoimmune encephalomyelitis (EAE). Breakdown of epithelial barriers increases intestinal permeability and systemic dissemination of microbiota-derived molecules. However, whether the gut-vascular barrier (GVB) is altered during EAE has not been reported. Here, we demonstrate that endothelial cell proliferation and vessel permeability increase before EAE clinical onset, leading to vascular remodeling and expansion of intestinal villi capillary bed during disease symptomatic phase in an antigen-independent manner. Concomitant to onset of angiogenesis observed prior to neurological symptoms, we identify an increase of intestinal perivascular immune cells characterized by the surface marker lymphatic vessel endothelial hyaluronic acid receptor 1 (LYVE-1). LYVE-1$^+$ is expressed more frequently on B cells that show high levels of CD73 and have proangiogenic properties. B cell depletion was sufficient to mitigate enteric blood endothelial cell proliferation following immunization for EAE. In conclusion, we propose that altered intestinal vasculature driven by a specialized LYVE-1$^+$ B cell subset promotes angiogenesis and that loss of GVB function is implicated in EAE development and autoimmunity.

1. Introduction

Biological barriers are essential to protect the host from noxious environment stimuli and play a pivotal role in maintaining homeostasis. Among these barriers, the gut is constantly challenged by trillions of intestinal microbes and environmental antigens. Defects of this multi-layer system are thought to be involved in a broad range of inflammatory and autoimmune diseases [1–6]. A growing body of evidence indicates that alteration of intestinal homeostasis is involved in the pathogenesis of multiple sclerosis (MS), a common chronic inflammatory and demyelinating disease of the central nervous system (CNS) [7–12].

Impairment of intestinal barrier integrity was previously estimated to occur in up to three-quarters of persons with MS (pwMS), leading to low-grade translocation of foreign and microbial antigens or microbes from the lumen into the intestinal lamina propria (LP) [13–16]. This process further increases inflammation and alters fine-tuned immunological balance, possibly promoting a breach of immune tolerance [17–19]. An association between inflammatory bowel disease (IBD) and MS has been described with a risk ratio of 1.54 for IBD and MS co-morbidity, and up to two-thirds of pwMS develop gastrointestinal complications, among which one-third reported intestinal symptoms before the first clinical episode suggestive of MS [20–22]. Several studies have shown an alteration of the intestinal microbiota in pwMS, including changes in bacterial strains that produce immunomodulatory metabolites (e.g., short-chain fatty acids) [9,10,12,23–31]. Consistently, modification of intestinal immune cell composition, including reduced dendritic cells and regulatory CD4 T cells was reported in the early stages of MS, and pwMS harbored increased intestinal permeability in the active phase of the disease [32,33]. However, it is still unclear whether intestinal alteration represents a pathological trigger or if it is a consequence of neurological disease progression [34]. A widely used

* Corresponding author. Laboratories of Neuroimmunology, Department of Clinical Neurosciences, Lausanne University Hospital and University of Lausanne, Chemin des Boveresses 155, 1066, Epalinges, Switzerland.
E-mail address: caroline.pot-kreis@chuv.ch (C. Pot).

https://doi.org/10.1016/j.jaut.2024.103292
Received 6 February 2024; Received in revised form 28 June 2024; Accepted 15 July 2024
Available online 26 July 2024

animal model of MS is experimental autoimmune encephalomyelitis (EAE). Mice with EAE display extensive alteration of intestinal milieu prior to neurologic symptom onset, thus favoring the first hypothesis [35,36]. Presymptomatic intestinal changes in EAE include increased intestinal permeability (that worsens with disease progression), dysbiosis, morphological changes such as increased villus length and crypt depths, increased cell density in the small intestine, inflammation, and infiltration of pro-inflammatory immune cells in intestinal LP [35–38]. Altogether, these studies indicate a substantial shift of intestinal milieu toward an inflamed state, including disruption of intestinal barrier functions. This loss of barrier function contributes to bacterial translocation and systemic dissemination of microbial-derived products, such as lipopolysaccharide (LPS), detected at high titers in blood and CNS of mice during symptomatic EAE [8]. An elevation in LPS serum level also occurs in pwMS [39]. Together, those data indicate that during EAE, intestinal homeostasis and barrier functions are disturbed before disease onset and potentially promote key pathological steps in development of neuroinflammation.

Systemic dissemination of microbial-derived macromolecules in neuroinflammation implies that intestinal barrier dysfunction is not limited to the epithelial-based barrier but also affects the recently discovered gut-vascular barrier (GVB) [40]. Primarily composed of endothelial cells, with the support of pericytes and enteric glial cells, the GVB shares morphological similarities with the BBB and controls macromolecule entry from LP into systemic circulation with a permeability estimated of 4 kDa [41]. Plasmalemma vesicle-associated protein (PLVAP, also known as PV-1) finely regulates intestinal blood endothelial cell (BEC) permeability, and its expression correlates with vascular permeability [42]. Interestingly, intestinal BEC transcriptome was highly enriched in genes related to angiogenesis following *Salmonella typhimurium* infection, known to induce GVB disruption [43]. Intestinal vasculature dysfunction is considered a critical factor in IBD pathogenesis, with patients demonstrating an activated endothelium, increased blood vessel density, and pathological angiogenesis [44,45]. Furthermore, results from the dextran sulfate sodium (DSS)-induced colitis model of IBD demonstrate microvascular remodeling, angiogenesis, and profound vascular leakage before epithelial barrier alteration, suggesting that GVB is negatively impacted by chronic intestinal inflammation [46–48]. Interestingly, a link between GVB and closing of the choroid plexus barrier mediated by gut-derived inflammatory mediators was recently proposed in DSS-induced colitis, suggesting a vascular axis between the intestine and the brain [49].

However, it remains unclear whether abnormal intestinal permeability during EAE is caused by alteration of the GVB and, if so, at what stage of disease. We here report a remodeling of the small intestinal vasculature, starting during preclinical phase of EAE, highlighted by increased vessel diameter, vascular permeability and EC proliferation, yielding an expansion of the capillary bed network at the disease peak suggestive of GVB disruption. We observe an expansion of intestinal proangiogenic, perivascular B cells expressing the ecto-5′-nucleotidase CD73 and hyaluronan receptor lymphatic vessel endothelial hyaluronan receptor 1 (LYVE-1). In addition, LYVE-1$^+$ B cells promote angiogenesis *in vitro* and participate in GVB disruption in mice immunized for EAE. We thus propose that this process could participate in immune tolerance breakdown.

2. Materials and methods

2.1. Mice

Wild-type mice were obtained from Charles-River Laboratories or bred in the animal facility. All mouse strains were on a pure C57BL/6J background. 8-12 weeks-old-mice were used for all experiments. Animals were kept in a specific pathogen-free (SPF) facility at Lausanne University. All experiments were carried out in respect with guidelines from the Cantonal Veterinary Service of the state of Vaud.

2.2. EAE induction

For the induction of active EAE, female mice were immunized with 100 μg myelin oligodendrocyte glycoprotein peptide 35–55 (MOG_{35-55}, Neobiotech, Clinisciences [previously Anawa], France) emulsified in complete Freund's adjuvant (CFA, 77140, Thermofisher, USA) supplemented with *Mycobacterium tuberculosis* H37Ra (BD0231141, BD Difco, USA) to a final concentration of 5 mg/ml. 200 μl of emulsion was subcutaneously injected into four sites on the flanks of mice. On days 0 and 2, after initial MOG_{35-55} injections, mice received intravenous injections of 100 ng pertussis toxin (P2980, Sigma-Aldrich, UK). Mice were weighed and scored daily using the following system: 0: no symptom, 1: tail paralysis, 2: hind limb paresis, 2.5: partial hind limb paralysis, 3: complete hind limb paralysis, 4: forelimb paresis and complete hind paralysis, 5: moribund or dead.

2.3. Larazotide acetate treatment

For larazotide acetate (LA) treatment, experiments were performed as previously described [5]. Briefly, EAE mice and unimmunized control mice received 50 μg of LA (SML2475, Sigma-Aldrich, Israel) in a volume of 150 μl or 150 μl of water as vehicle control, respectively, twice a day by oral gavage starting on the day of immunization and continuously throughout the experiment.

2.4. Whole-mount immunostaining and vessel morphometric analysis

Whole-mount immunostaining was performed as previously described [50]. Briefly, mice were perfused with 4 % paraformaldehyde and the intestines were fixed in a picric acid fixation buffer (P6744, Sigma-Aldrich, Switzerland). Jejunum immunostaining was performed with DAPI (4′,6-diamidino-2-phenylindole, dil: 1:4000) and the following primary antibodies: goat anti-mouse VEGFR2 (dil 1/100, polyclonal, AF644, R&D systems, USA), rabbit anti-mouse LYVE-1 (dil: 1/400, polyclonal, 11–034, AngioBio, USA), rat anti-mouse B220 (dil: 1/400, clone: RA3-6B2), Goat anti-mouse IgA (dil: 1/200, polyclonal, 1040-01, SouthernBiotech, USA), rat anti-mouse F4/80 (dil: 1/200, clone: BM8, MF48000, Invitrogen, USA), and secondary antibodies, donkey anti-rabbit IgG (H + L) AF647 (dil: 1/500, A-31573, Invitrogen, USA), donkey anti-goat IgG (H + L) AF555 (dil: 1/500, A-11055, Invitrogen, USA), goat anti-Syrian Hamster IgG (H + L) AF 488 (dil: 1/500, A-21110, Invitrogen, USA), donkey anti-Rat IgG (H + L) AF488 (dil: 1/500, A-21208, Invitrogen, USA). Image acquisition was performed on a Zeiss LSM 880 confocal microscope, and image analysis and 3D reconstruction were performed using Fiji software. Morphometric analysis was performed with Angiotools software [51].

2.5. Isolation of intestinal leukocytes and endothelial cells

Immune cells from small intestine LP were isolated as previously described [35]. Briefly, the jejunum section of the small intestine was opened longitudinally and washed three times in 1x phosphate-buffered saline (PBS). Washed intestine was cut into 2 cm pieces and first incubated for 20 min at 37 °C in Hanks' Balanced Salt solution (HBSS, 14170-112, Gibco, USA) containing 10 mM EDTA (46-034-CI, Corning, USA) at 80 rpm. Tissues were washed twice by vortexing in 1x PBS and jejunal pieces were then incubated in a dissociating mix composed of 5 mL HBSS, DNAse I recombinant (1U/mL, 04716728001, Roche, Germany), 2 % fetal calf serum (FCS, Biowest, France) and Liberase TL (1 Wünsch unit/mL, 05401020001, Roche, Germany) for 20 min at 37 °C. Enzymatic dissociation was performed 2 times for immune cells isolation or 3 times for endothelial cells isolation. The remaining tissue pieces were mechanically dissociated on a 70 μm cell strainer using a syringe plunger. The cellular suspensions were then washed with HBSS complemented with 10 % FCS, filtered through 40 μm cell strainer and resuspended in complete culture medium for further analysis.

2.6. Isolation of CNS immune cells

Mice were perfused through the left ventricle with ice-cold 1x PBS, the brains were dissected, and spinal cords were collected by flushing the vertebral canal with ice-cold 1x PBS. CNS tissue was then cut into pieces and digested in Dulbecco's Modified Eagle Medium (DMEM, 41965039, Gibco, UK) supplemented with 2.5 mg/ml collagenase D (11088858001, Sigma-Aldrich, Germany) and DNAse 1 at 1 mg/ml (10104159001, Sigma-Aldrich, Germany) for 45 min at 37 °C. Mononuclear cells were isolated by passage through 70 μm cell strainer, followed by Percoll gradient centrifugation (70 %/37 %). Leukocytes were removed from the interphase, washed, and resuspended in culture medium for downstream analysis.

2.7. Flow cytometry and cell sorting

Single-cell suspensions were washed twice in 1x PBS and stained with LIVE/DEAD fixable red viability dye (L23102, Invitrogen, USA) according to the manufacturer's instructions. For extracellular staining, cells were first incubated with anti-CD16/32 antibody (clone: 93, 16-0161-85, Invitrogen, USA) in fluorescence-activated cell sorting (FACS) buffer (1x PBS containing 1 % BSA) and stained with anti-mouse fluorochrome-conjugated antibodies: CD45 (clone: 30-F11, 103138, USA), CD31 (clone: 390, 102418, USA), Podoplanin/gp38 (clone: 8.1.1, 127410, USA), PLVAP (clone: MECA-32, 120505, USA), B220 (clone: RA3-6B2, 103236, USA), CD73 (clone: TY/11.8, 127205, USA) purchased from Biolegend, CD64 (clone: X54-5/7.1, 12-0641-82, USA), LYVE-1 (clone: ALY7, 48-0443-82, USA), F4/80 (clone: BM8, 56-4801-82, USA), CD19 (clone: 1D3, USA), CD11c (clone: N418, 117318, USA), CD11b (clone: M1/70, 101226, USA) purchased from eBioscience at 4 °C for 30 min. For intracellular staining, cells were fixed and permeabilized using Foxp3/transcription factor staining Buffer set (00-5523-00, eBioscience, USA) and stained intracellularly with labeled antibody rat anti-IgA (clone: 11-44-2, 1165-02, SouthernBiotech, USA) for 30 min at RT. Data were acquired on an LSR II-cytometer and analyzed using FlowJo software.

2.8. Intestinal vascular permeability assay

Intestinal vascular permeability was assessed using the Evans blue dye method adapted from previous publication [52]. Mice received an intravenous injection of 100 μl of Evans blue (E2129, Merck, India) solution at 0.5 % (w/v) at 7 days post-immunization (DPI). Mice were sacrificed 10 min after Evans blue injection and perfused with 10 ml of PBS. The jejunum part of the small intestine tissues was removed, opened longitudinally, and feces removed. Photographs were taken, tissues were blotted dry, and Evans blue dye was extracted with 500 μl of formamide (47671, Sigma-Aldrich, Germany) overnight at 60 °C. Evans blue concentration was then measured by spectrophotometry at 600 nm.

2.9. Aortic ring assay co-cultures

Aortic ring co-culture assay was adapted from previous publications [53,54]. Aortae were isolated from wild-type C57BL/6 J mice, flushed with 1xPBS, cut into 0.5 mm thick rings, and incubated in serum-free culture media (DMEM) complemented with gentamicin (G1272-100 ml, Sigma-Aldrich, Israel), non-essential amino acids (11140-035, Gibco, UK), sodium pyruvate (S8636-100 ml, Sigma-Aldrich, Japan) overnight at 37 °C and 5 % CO_2. Aortic rings were embedded in growth factor reduced matrigel (354230, Corning, USA), and cultivated in 100 μl of complete media (DMEM complemented with 10 % FCS, gentamicin, non-essential amino acids, and sodium pyruvate) in the presence of 20 ng/ml basic fibroblast growth factor (bFGF) (F0291, Sigma-Aldrich, USA) during 3 days at 37 °C and 5 % CO_2. After 3 days, wells containing aortic rings were washed with a complete medium before adding freshly FACS-sorted LYVE-1^+ or LYVE-1^- B cells. Medium only [non-stimulated (NS) condition] or completed with 20 ng/ml of bFGF (bFGF condition) were added to the aortae for negative and positive control, respectively.

To obtain B cells, EAE was induced in wild-type C57BL/6 J female mice, and at 7 DPI, siLP immune cells were extracted and fluorescence-activated cells sorted into $CD45^+$ $CD11b^-$ $F4/80^-$ $B220^+$ LYVE-1^+ and $CD45^+$ $CD11b^-$ $F4/80^-$ $B220^+$ LYVE-1^- populations. Co-cultures were performed by adding 70 000 LYVE-1^+ or LYVE-1^- B cells per well and images were acquired daily using Leica DMi1 Inverted Microscope to assess the sprouting area. A blinded investigator performed the quantification of the sprouting area with Fiji software.

2.10. B cell depletion therapy

Treatment with the mouse monoclonal anti-CD20 (clone: MB20-11, BE0356, InVivoMAb, USA) or with the mouse IgG2c isotype control (BE0366, InVivoMAb, USA) was performed as previously described [55]. Antibodies were administered intravenously (250 μg/mice) once in unimmunized control mice and seven days before EAE induction in the group of mice with EAE. Immune cells were isolated from the spleen and the duodenum LP at 7 DPI to control for B cell depletion, while endothelial cells were extracted from jejunum LP to perform flow cytometry analysis.

2.11. RT-qPCR

Total RNA was extracted using the RNeasy Mini Kit (74104, Qiagen, Germany) according to the manufacturer's protocol. cDNA was produced from RNA without amplification using the Superscript II RT (18064014, Invitrogen, USA). PCR products were amplified with the PowerUp SYBR Green Master Mix (A25742, Applied Biosystem, Lithuania). Samples were analyzed using the StepOne Real-Time PCR System. Glyceraldehyde 3-phosphate dehydrogenase (*Gapdh*) was used as reference genes, and the comparative $2^{-\text{Delta CT}}$ method was employed to evaluate the relative mRNA expression of the gene of interest. Primers were purchased from Microsynth AG (Balgach, Switzerland). The following primers were used: *Gapdh* (forward) 5′-TGT GAA CGG ATT TGG CCG TA-3′, (reverse) 5′-ACT GTG CCG TTG AAT TTG CG-3′, *CCND3* (forward):5′-CGT CGC TTC TCC TAG GAC TC-3′, (reverse) 5′-AAC ACA GCA GCT CCA TCC TG-3′, *Eng* (forward) 5′-TTC TCA CAC ACG TGG CCC-3′, (reverse) 5′-AAC ACA GCA GCT CCA TCC TG-3'.

2.12. RNA-sequencing

EAE was induced in wild-type C57BL/6J female mice as described above. At 7 DPI, the siLP was extracted and cells were FACS sorted into Viable $CD45^+$ $CD11b^-$ $F4/80^-$ $CD11c^-$ $B220^+$ LYVE-1^+ population and Viable $CD45^+$ $CD11b^-$ $F4/80^-$ $CD11c^-$ $B220^+$ LYVE-1^- population before RNA extraction. The RNA-seq was performed in The Lausanne Genomic Technologies Facility. RNA quality was assessed on a Fragment Analyzer (Agilent Technologies), and all RNAs had an RQN between 7.7 and 9. RNA-seq libraries were prepared from 10 ng of total RNA with Takara SMART-seq v4 PLUS kit following the manufacturer's protocols. Libraries were quantified by a fluorometric method (QubIT, Life Technologies) and their quality assessed on a Fragment Analyzer (Agilent Technologies).

Gene set enrichment analysis (GSEA) was performed with the pre-ranked gene list function of GSEA software from the UC San Diego and Broad Institute using the t-statistic to rank the input gene lists [56,57]. MTORC1 signaling, oxidative phosphorylation and inflammatory response were assessed using the hallmark gene set collection from the Molecular Signatures Database (MSigDB) [58]. Cell cycle was assessed using Kyoto Encyclopedia of Genes and Genomes (KEGG) collection. Activation of immune response and positive regulation of cytokine production involved in immune response were assessed using the Gene Ontology Biological Process (GO: BP) collection.

2.13. Statistics

Data analyses and graphs were performed using the GraphPad Prism software for Windows (GraphPad Software Inc., San Diego, CA, USA). A P-value <0.05 was considered as significant. Statistical tests used in this study include two-tailed Mann-Whitney *U* test, two-tailed unpaired Student t-test, ordinary one-way ANOVA with Tukey's multiple comparisons test or Holm-Šídák's multiple comparisons test, or two-way ANOVA with Šídák's multiple comparisons test as specified in the figure's legends. We performed PCA on the gene expression data while accounting for paired samples within Python (v 3.7.7). We first removed the paired sample effect with ordinary least squares regression using the 'ols' function within statsmodels (v0.13.0), and then we performed PCA using the 'PCA' function within scikit-learn (v1.0.2). The sample size for each experiment is specified in the figure's legends.

Preprocessing and statistical analysis of the RNA-seq were performed by the Lausanne Genomic Technologies facility with R (R version 4.1.0). For data processing, purity-filtered reads were adapters and quality trimmed with Cutadapt (v. 1.8, [59]). Reads matching to ribosomal RNA sequences were removed with fastq_screen (v. 0.11.1). Remaining reads were further filtered for low complexity with reaper (v. 15–065, [60]). Reads were aligned against the Mus_musculus.GRCm38.102 genome using STAR (v. 2.5.3a, [61]). The number of read counts per gene locus was summarized with htseq-count (v. 0.9.1, [62]) using Mus_musculus. GRCm38.102 gene annotation. Quality of the RNA-seq data alignment was assessed using RSeQC (v. 2.3.7, [63]). Statistical analysis was performed for genes independently in R (R version 4.1.0). Genes with low counts were filtered out according to the rule of 1 count(s) per million (cpm) in at least 1 sample. Library sizes were scaled using TMM normalization. Subsequently, the normalized counts were transformed to cpm values and a $\log_2$ transformation was applied by means of the function cpm with the parameter setting prior.counts = 1 (EdgeR v 3.34.1; [64]). After data normalization, a quality control analysis was performed through hierarchical clustering and sample PCA (plots of first two principal components). The samples cluster correctly by experimental group. After taking paired samples into account (using the function removeBatchEffect(k) from the R Bioconductor package limma), the separation of the two groups is even better than in the unsupervised case. Differential expression was computed with the R Bioconductor package limma by fitting data to a linear model [65]. The approach limma-trend was used. Fold changes were computed, and a moderated *t*-test with paired samples was applied to compare the two conditions. P-values were adjusted using the Benjamini-Hochberg (BH) method, which controls for the false discovery rate (FDR).

Ethics approval

All experiments were performed in accordance with guidelines from the Cantonal Veterinary Service of state Vaud (authorizations #VD3767 and #VD3393)

3. Results

3.1. Morphological changes in intestinal vasculature occur at the presymptomatic phase of EAE disease

Small intestinal villi morphology alteration during neuroinflammation was previously described [36], however the specific features are not clearly identified. Furthermore, impact of EAE on enteric endothelium is poorly understood. To better describe these changes, we performed whole-mount immunostaining of intestinal tissues by staining for vascular endothelial growth factor receptor 2 (VEGFR2), a key angiogenesis player widely expressed in endothelial cells [66]. We focused our analysis on the jejunum midsection of the small intestine, whose morphology is significantly affected during EAE [36]. To evaluate the impact of immunization on intestinal vasculature, we immunized a group of wild-type mice with the antigen myelin oligodendrocyte glycoprotein 35-55 ($MOG_{35–55}$) emulsified with complete Freund's adjuvant (CFA) subcutaneously into flanks. Pertussis toxin was injected intravenously (IV) at days 0 and 2. The control group consisted of age- and sex-matched unimmunized mice. Only immunized mice developed neurological symptoms (Fig. 1A). We chose two different time points during EAE disease course to analyze intestinal capillary bed architecture: EAE disease peak (day 15) (closed arrow and representative images Fig. 1B) and 7 days post-immunization (DPI), a time prior to symptom onset (Fig. 1A open arrow and representative images Fig. 1C).

We observed that the vascularized area of the villus capillary bed was enlarged in mice at the peak of EAE compared to age-matched unimmunized control mice (Fig. 1B–D). These results were in accordance with the significant increase in cumulative vessel length observed in mice at the peak of disease compared with unimmunized mice (Fig. 1E). Vessel morphometric analysis further showed a significant increase in vessel branching in mice with EAE compared to unimmunized mice (Fig. 1F). However, vessel diameter was similar between unimmunized and EAE mice at this time point (Fig. 1G).

We and others have shown that intestinal LP inflammation is increased at the presymptomatic EAE stage [35,36,67]. We thus aimed to determine whether vascular remodeling appears early in disease development and performed a similar analysis as described above at 7 DPI (Fig. 1C, left panels). At this time point, no difference was observed in the villus vascular bed area (illustrative Fig. 1C and quantification in Fig. 1H), total blood vessel length (Fig. 1I) and number of vessel branchpoints between the two mice groups (Fig. 1J). However, we observed a significant increase in vessel diameter in mice immunized for EAE compared to the unimmunized control group (illustrative image Fig. 1C right panels, and quantification 1K). Together, these results suggest that vascular remodeling occurs and is initiated in the intestine prior to disease onset characterized by vessel enlargement. We propose that restructuring existing vessels precedes generation of an enlarged and more complex villi capillary network that we observe in mice with neurological symptoms.

3.2. Intestinal angiogenesis and vascular permeability increase during the presymptomatic EAE

Vessel enlargement is observed during pathological angiogenesis and is associated with increased vascular permeability, therefore we aimed to address whether at 7 DPI intestinal endothelium displays increased proliferation and vascular leakage [68–70]. Not only increased vessel diameter can result from inflammation-induced vasodilatation, but capillary enlargement can also be a precursor sign of angiogenesis. During chronic airway inflammation induced by *Mycoplasma pulmonis* infection capillary enlargement precedes the formation of new blood vessels [71]. To address whether vessel enlargement is related to the local proliferation of blood endothelial cells (BEC, $CD45^{-}CD31^{+}$podoplanin $[gp38]^{-}$), we extracted the small intestinal lamina propria (siLP) and assessed the numbers of BECs from unimmunized and EAE-induced mice at 7 DPI by flow cytometry quantification. We observed a significant increase in the number of BECs in the LP of the jejunum of mice 7 days after immunization compared to unimmunized mice (Fig. 2A and B representative FACS plots). This strengthens our hypothesis that angiogenesis happens before the first EAE symptoms despite lack of capillary bed area expansion. We then sorted BECs by flow cytometry from siLP of mice from both groups and performed quantitative real-time PCR. siLP BECs from mice immunized for EAE at 7 DPI expressed significantly higher levels of endothelial cell proliferation-associated genes *CCND3* (cyclin D3, Fig. 2C) and *Eng* (endoglin, Fig. 2D) than BEC isolated from control mice (BEC gating strategy Fig. S1A) [72]. siLP BEC also showed a significant upregulation of the ecto-5′-nucleotidase CD73 expression compared to unimmunized controls (Fig. 2E quantification and gating Fig. S1B). CD73 induces endothelial cell sprouting and promotes blood vessel permeability [73].

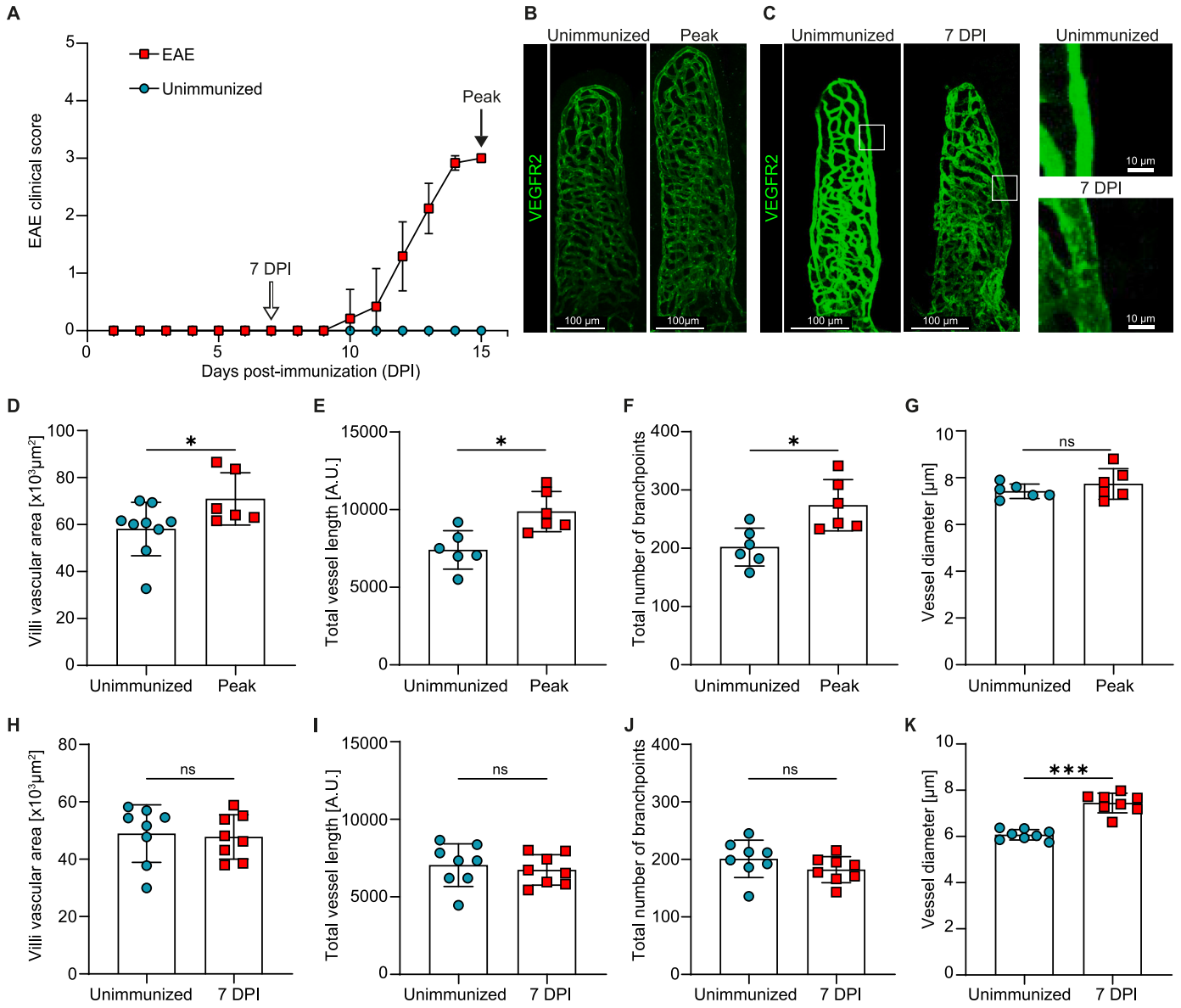

Fig. 1. Morphological remodeling of the small intestine vasculature during EAE. **(A)** EAE disease course (n = 6–9 mice per group), arrows indicate the two time-points (open arrow: 7 DPI and closed arrow: 15 DPI for disease peak) at which intestinal vasculature was analyzed. **(B)** Representative whole-mount immunofluorescence images of jejunum vasculature from unimmunized mice (left panel) and from mice at EAE peak (right panel) stained for VEGFR2. Scale bars represent 100 µm. **(C)** Representative whole-mount immunostaining images of jejunum from unimmunized (left panel) and EAE-induced mice at 7 DPI (middle panel) stained for VEGFR2. Scale bars represent 100 µm. Squares indicate the area shown at higher magnification to highlight changes in capillary diameter between unimmunized (top right panel) and mice immunized for EAE at 7 DPI (bottom right panel). Scale bars represent 10 µm. Quantification of **(D)** villi vascular bed area, **(E)** cumulative vessel length per villus, **(F)** number of vessel branchpoints per villus, and **(G)** capillary diameter of unimmunized mice and mice at EAE peak (n = 6–9 mice per group, at least 8 villi quantified per biological replicate). Quantification of **(H)** villi vascular bed area, **(I)** cumulative vessel length per villus, **(J)** number of vessel branchpoints per villus, and **(K)** capillary diameter of unimmunized or mice immunized for EAE at 7 DPI (n = 8 mice per group, at least 8 villi quantified per biological replicate). Data were combined from two experiments (D–K). Symbols represent biological replicates (D–K). Representative of two (H–K) or three (D–G) independent experiments. Mean ± SD. ns: not significant, *P ≤ 0.05 and ***P ≤ 0.001. Data were analyzed by a two-tailed Mann-Whitney test (D–K).

Moreover, siLP BECs express PLVAP, a marker of increased vascular permeability and GVB injury [74–76]. PLVAP is further related to angiogenesis and promotes leukocyte migration [77,78]. The number of PLVAP$^+$ BECs was significantly increased by ~2.3-fold in immunized compared to control mice (Fig. 2F, illustrative FACS plots Fig. 2G and gating Fig. S1C), indicating increased capillary permeability. Furthermore, small intestinal vascular permeability was evaluated *in vivo* using the Evans blue method [52,79]. Extravasation of Evans blue dye into small intestinal tissues was significantly increased in mice immunized for EAE at 7 DPI compared to unimmunized controls following a systemic injection of Evans blue (Fig. S1D quantification and S1E representative photographs).

To further evaluate the vascular compartment during presymptomatic EAE disease phase, lymphatic endothelial cells (LECs, CD45$^-$CD31$^+$podoplanin [gp38]$^+$) from the siLP were analyzed by flow cytometry. Unlike BECs, abundance of intestinal LECs was not modified in EAE-induced mice (Fig. 2H and B representative FACS plot). In addition, we performed morphologic analysis of lacteals, specialized lymphatic capillaries found in the small intestinal villi, by whole-mount immunostaining using the marker LYVE-1 [80]. We observed a similar lacteal length in unimmunized and mice immunized for EAE at 7 DPI (Fig. 2I). Furthermore, the lacteal surface area (Fig. 2J) was not altered

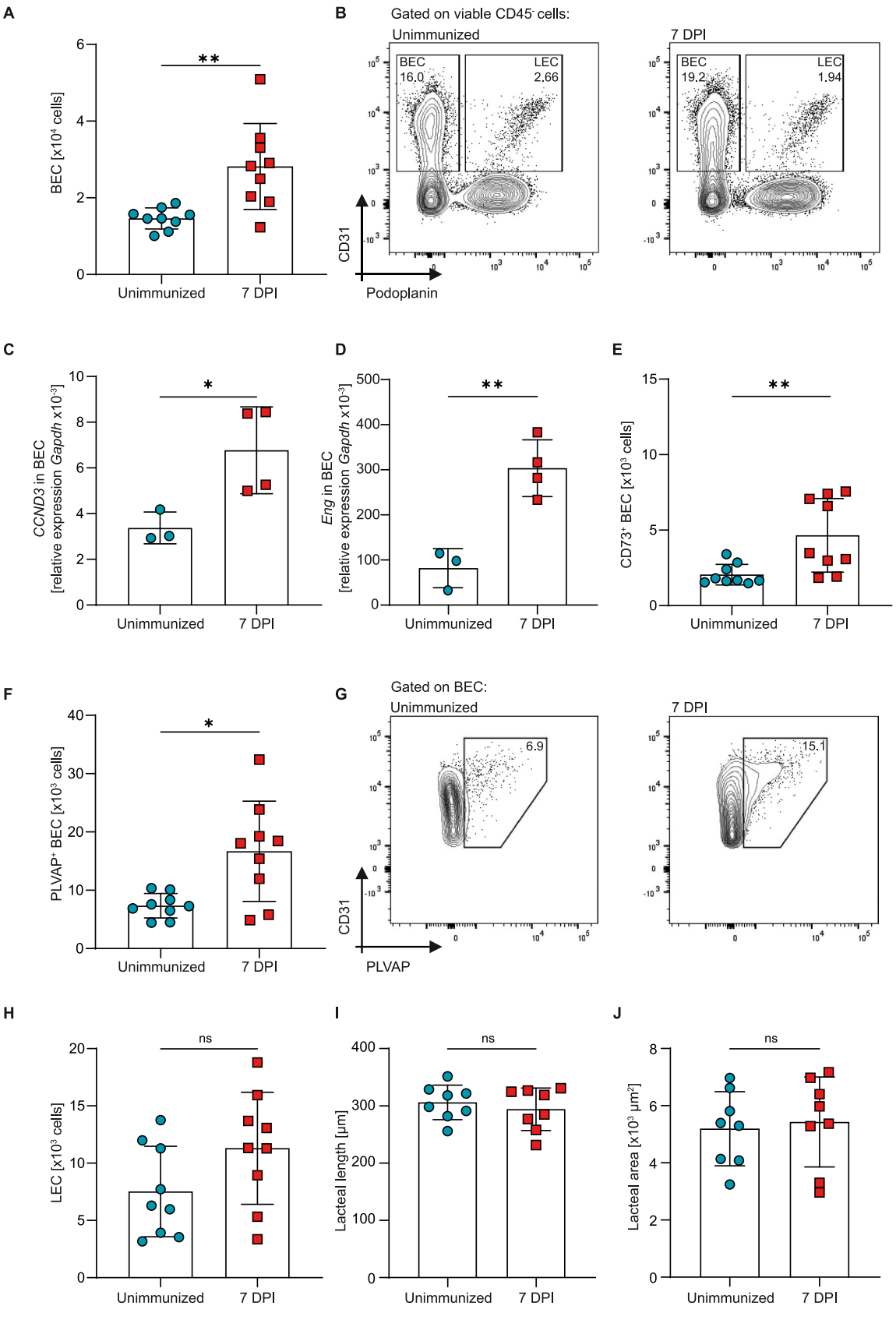

(caption on next page)

Fig. 2. Increase of proliferation and markers of vessel permeability in small intestinal blood endothelial cells manifest prior to EAE clinical onset. Quantification of **(A)** blood endothelial cell (BEC) absolute number evaluated by FACS in small intestinal lamina propria (siLP) and **(B)** representative FACS plot of BEC ($CD31^+podoplanin^-$) and lymphatic endothelial cell (LEC [$CD31^+podoplanin^+$]) gated on viable $CD45^-$ cells from unimmunized (B, left panel) or mice immunized for EAE at 7 DPI (B, right panel) (n = 9 mice per group). Expression of the proliferation-associated markers **(C)** *CCND3* (cyclin D3) and **(D)** *Eng* (endoglin) assessed by quantitative real-time PCR performed on total RNA extracted from sorted siLP BEC of unimmunized or mice immunized for EAE at 7 DPI. Count of **(E)** CD73-expressing and **(F)** PLVAP-expressing BECs (n = 9 mice per group) with **(G)** representative FACS plot of PLVAP staining in BEC from unimmunized (left panel) and EAE-induced mice at 7 DPI (right panel). **(H)** Quantification of LEC count evaluated by FACS in siLP of unimmunized mice and mice immunized for EAE at 7 DPI (n = 9 mice per group). Quantification of **(I)** lacteal (lymphatic capillary of the small intestine) length and **(J)** lacteal area assessed in unimmunized mice and mice immunized for EAE at 7 DPI by whole-mount immunofluorescence based on LYVE-1 staining (n = 8 mice per group). Data were combined from two experiments (A, E, F, H, I, J). Symbols represent biological replicates (A–J). Mean ± SD. ns: not significant, *P ≤ 0.05 and **P ≤ 0.01. Data were analyzed by a two-tailed Mann-Whitney test (A–J) and are representative of two (C, D, H, I, J) or three (A, E, F) independent experiments.

in mice EAE-induced compared to unimmunized control mice, indicating a conserved lacteal architecture in immunized mice. Altogether, these results indicate that intestinal BECs, but not LECs, actively proliferate and harbor markers associated with increased vascular permeability and GVB destabilization in mice immunized for EAE prior to clinical onset, resulting in increased intestinal vascular permeability *in vivo*.

3.3. Expansion of perivascular LYVE-1-expressing hematopoietic cells in siLP following EAE induction

We then investigated which factors promote angiogenesis in the siLP during EAE. When examining the lymphatic vasculature of the siLP by whole-mount immunostaining, we observed expansion of round-shaped, individual cells expressing LYVE-1 (nonvascular $LYVE\text{-}1^+$ cells) in mice from the EAE-induced group (Fig. 3A). Although a *bona fide* marker of LECs, LYVE-1 is also expressed by M2-like perivascular macrophages during development and in tumor microenvironment, as well as in adult dental pulp and adipose tissues with proangiogenic properties [81–83]. Furthermore, perivascular CNS border-associated macrophages express LYVE-1 in homeostatic and inflammatory conditions, including EAE [84, 85]. Based on previous studies, we assessed the positioning of nonvascular $LYVE\text{-}1^+$ cells in relation to blood capillaries and found that they were in close proximity to or in direct contact with the intestinal microvasculature (Fig. 3B and Movie S1 for three-dimensional reconstitution), indicative of a perivascular phenotype. Quantifying nonvascular $LYVE\text{-}1^+$ cells showed significantly increased $LYVE\text{-}1^+$ cell abundance in the siLP of mice immunized for EAE mice compared to the control group (Fig. 3C). We then asked if they were detected in hematopoietic $CD45^+$ cells by flow cytometry. There were significantly more LYVE1-expressing $CD45^+$ hematopoietic cells in the siLP of mice immunized for EAE compared to control mice (Fig. 3D and E), confirming their expansion at an early time point of EAE and revealing their hematopoietic origin.

Supplementary video related to this article can be found at https://doi.org/10.1016/j.jaut.2024.103292

Next, we sought to identify the $CD45^+LYVE\text{-}1^+$ perivascular population by analyzing the expression of myeloid and lymphoid cell-specific markers. In EAE-induced mice at 7 DPI, $CD45^+LYVE\text{-}1^+$ cells were segregated into at least three different subpopulations. 60.5 ± 19.1 % of $CD45^+$ $LYVE\text{-}1^+$ cells expressed the pan B cell marker B220 (Fig. 3F illustrative FACS plot and quantification Fig. 3I). Consistent with a report indicating the presence of intestinal $LYVE\text{-}1^+$ macrophages, 19 ± 10.9 % of the $CD45^+LYVE\text{-}1^+$ cells expressed the myeloid-associated marker CD11b, and the macrophage-associated markers CD64 (FcγRI) and F4/80 (Fig. 3G illustrative FACS plot and quantification Fig. 3I) [86]. Finally, 10.7 ± 7.5 % of the remaining $CD45^+LYVE\text{-}1^+$ cells expressed Immunoglobulin A (IgA) (Fig. 3H illustrative FACS plot and quantification Fig. 3I). This indicates that a large proportion of $CD45^+LYVE\text{-}1^+$ immune cells are B cells. Altogether, these results show an intestinal expansion of perivascular immune cells, including macrophages, B cells, and IgA^+ plasmablasts, characterized by expression of LYVE-1 concomitant with BEC proliferation and vascular remodeling.

3.4. Gut-specific expansion of $LYVE\text{-}1^+$ B cells and macrophages in EAE-induced mice

Having established that different subpopulations of $CD45^+LYVE\text{-}1^+$ cells accumulate in the jejunum before the first neurological clinical signs, we then aimed to monitor their changes in the siLP at steady-state and in mice at 7 DPI by flow cytometry. The frequency of $LYVE\text{-}1^+$ macrophages was significantly increased by two-fold after immunization, yielding a proportion of 2.6 % of the total siLP $CD45^+$ immune cells (Fig. 4A illustrative FACS plot and Fig. 4B quantification). We corroborated this finding by whole-mount immunostaining showing the co-localization of LYVE-1 and F4/80 (Fig. 4C), confirming the presence of LYVE-1-expressing macrophages. In addition, we found that $LYVE\text{-}1^+$ IgA^+ plasmablasts, likely arising from $LYVE\text{-}1^+$ B cells undergoing activation and differentiation, were significantly expanded following MOG immunization (Fig. 4D illustrative FACS plot and Fig. 4E quantification), representing 1.8 % of the total intestinal $CD45^+$ immune cells at 7 DPI. IgA-expressing $LYVE\text{-}1^+$ immune cells were also identified by immunofluorescence (Fig. 4F). In agreement with our previous findings, $CD45^+LYVE\text{-}1^+B220^+$ cells ($LYVE\text{-}1^+$ B cells) represent the largest increased cell subset following immunization with a 3.5-fold increase compared to non-immunized mice, rising from 1.9 % to 7 % of the total intestinal $CD45^+$ immune cells (Fig. 4G illustrative FACS plot and Fig. 4H quantification). Co-localization of B220 and LYVE-1 surface expression was confirmed by immunofluorescence analysis on intestinal tissue of mice immunized for EAE at 7 DPI (Fig. 4I). Since the surface marker B220 is also expressed in thymocytes and natural killer (NK) cells, we confirmed by flow cytometry that all $B220^+LYVE\text{-}1^+$ express the specific B cell marker CD19 (Fig. 4J and illustrative FACS plot Fig. 4K), corroborating that $LYVE\text{-}1^+$ immune cells encompass *bona fide* B cells. We then asked if expansion of $LYVE\text{-}1^+$ B cells was specific or reflected an increase in the whole enteric B cell population. We did not observe an expansion of total B cells in intestinal tissues at 7 DPI (Fig. 4L), demonstrating a specific expansion of $LYVE\text{-}1^+$ B cells.

We then wondered if $LYVE\text{-}1^+$ B cells could be detected in other organs, and we first explored their presence in the spleen, which could reflect an increase in circulating $LYVE\text{-}1^+$ B cells. Splenic B cells at 7 DPI did not express LYVE-1 (Fig. 4M). This suggests a gut-specific expansion of LYVE-1-expressing B cells in siLP that would not result from circulating $LYVE\text{-}1^+$ B cells. Given the recent description of regulatory gut-derived IgA^+ B cells shown to infiltrate the CNS in pwMS and mice with EAE and the identification of $LYVE\text{-}1^+$ IgA^+ cells, we addressed whether $LYVE\text{-}1^+$ B cells are found in the CNS during neuroinflammation [87,88]. CNS-infiltrating immune cells were extracted at the peak of EAE, and the proportion of total $CD45^+LYVE\text{-}1^+$ immune cells was evaluated by flow cytometry. $CD45^+LYVE\text{-}1^+$ immune cells were not detected in the CNS during EAE. These data suggest an expansion of three subsets of LYVE-1-expressing immune cells, mainly driven by $LYVE\text{-}1^+$ B cells, specifically in the intestine following EAE immunization.

To address whether $LYVE\text{-}1^+$ cell expansion, as well as alteration of intestinal vasculature, are antigen-specific, we performed additional analysis in mice immunized with an emulsion of PBS and CFA with IV administration of pertussis toxin (PBS/CFA/PTX) versus mice

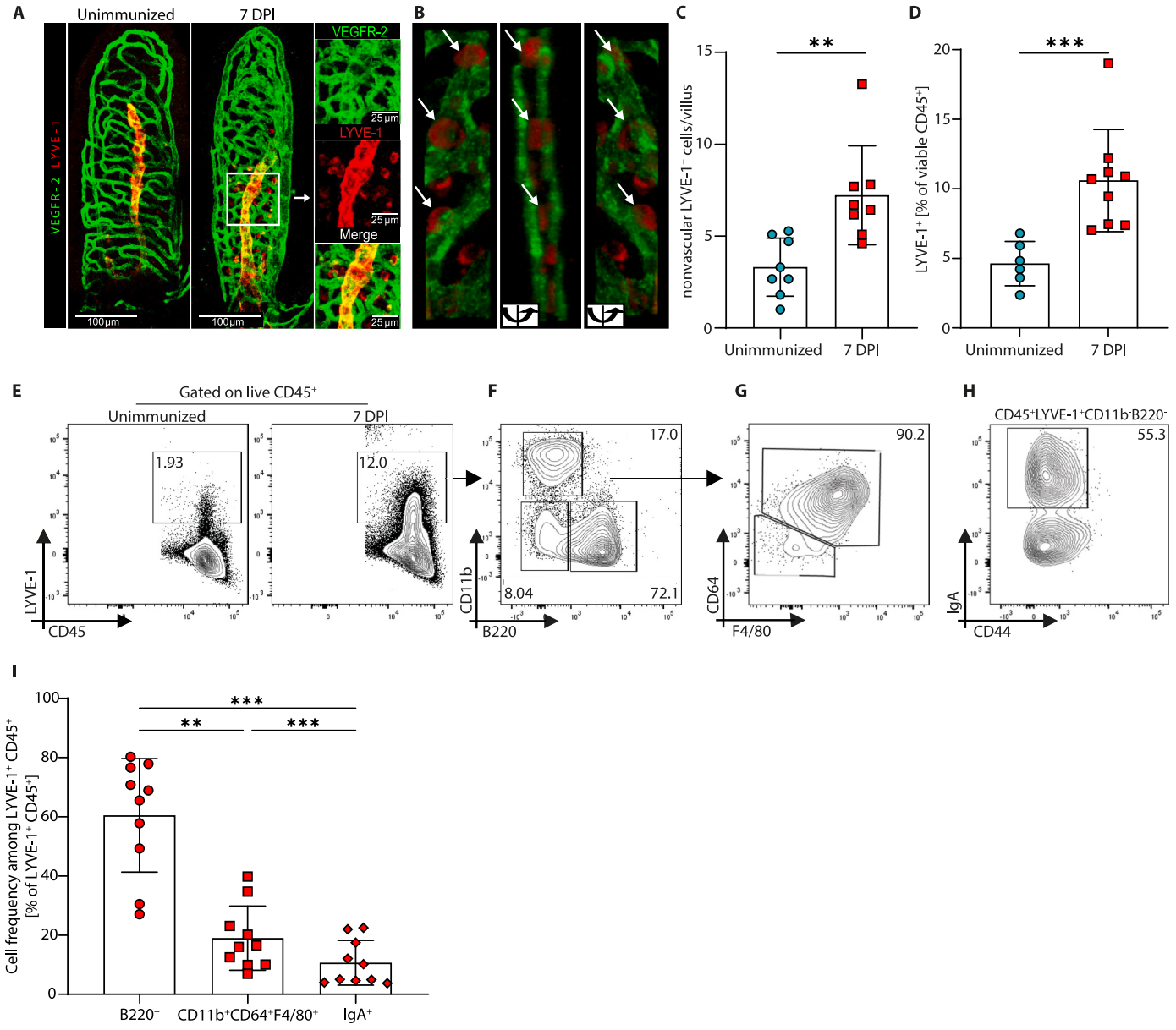

Fig. 3. Perivascular LYVE-1$^+$ immune cells are expanded in mice immunized for EAE and encompass macrophages, B cells, and IgA-positive cells. **(A)** Representative whole-mount immunostaining images of jejunum section from unimmunized (left panel) or mice immunized for EAE at 7 DPI (right panel) stained for VEGFR2 (green) and LYVE-1 (red). Squares indicate the area shown at higher magnification on the neighboring panel. Scale bars represent 100 µm (left and middle panels) or 25 µm (right panels). **(B)** Three-dimensional reconstruction of the whole-mount immunostaining of mice immunized for EAE at 7 DPI stained for VEGFR2 (green) and LYVE-1 (red). Arrows indicate nonvascular LYVE-1$^+$ cells in direct contact with blood capillaries. Each panel shows the same image with 90° rotation on the Y axis. **(C)** Quantification of nonvascular LYVE-1$^+$ cell (n = 8 mice per group, with at least 8 villi quantified per mice) from whole-mount immunostaining. Flow cytometric analysis of **(D)** the frequency of LYVE-1-expressing cells in the CD45 compartment (n = 6–9 mice per group) and **(E)** representative FACS plot of un-immunized (left panel) and mice undergoing EAE at 7 DPI (right panel). Identification by flow cytometry of LYVE-1 co-expression with **(F)** the pan-B cell marker B220 and the myeloid lineage marker CD11b, **(G)** macrophage-associated markers CD64 and F4/80, and **(H)** intestinal plasmablast marker immunoglobulin A (IgA). **(I)** Quantification of the cell frequency of B220$^+$ (as identified in F), CD11b$^+$CD64$^+$F4/80$^+$ (as identified in G), and IgA$^+$ (as identified in H) among CD45$^+$LYVE-1$^+$ isolated from siLP of mice immunized for EAE at 7 DPI. Data were combined from two experiments (C, D, and I). Symbols represent biological replicates (C, D, and I). Mean ± SD. **P ≤ 0.01 and ***P ≤ 0.001. Data were analyzed by two-tailed Mann-Whitney test (C–D) or one-way ANOVA with Tukey's multiple comparisons test (I) and are representative of two (C, I) or at least three (D) independent experiments.

immunized with the antigen MOG (MOG/CFA/PTX). Whole-mount immunostaining of the jejunum revealed a significant enlargement of blood capillary diameter in both PBS/CFA/PTX and MOG/CFA/PTX groups at 7 DPI compared to unimmunized controls (Fig. S2A). Additionally, there was a trend toward increased abundance of intestinal BECs (Fig. S2B) and vascular permeability (Fig. S2C) in mice immunized in both groups compared to unimmunized mice. Flow cytometry and whole-mount analysis of intestinal immune cell population showed a significant increase in nonvascular LYVE-1$^+$ cells (Fig. S2D). The frequency of LYVE-1$^+$ CD45$^+$ (Fig. S2E) and B220$^+$LYVE-1$^+$ (Fig. S2F) were similarly increased in mice that received PBS/CFA/PTX and MOG/CFA/PTX immunization compared to unimmunized mice. Together, those data indicate that change in intestinal vasculature and expansion of intestinal LYVE-1$^+$ B cells are not antigen-specific and are likely the result of CFA immunization. This is interesting as it could indicate broader mechanisms of breaking immune tolerance that take place in

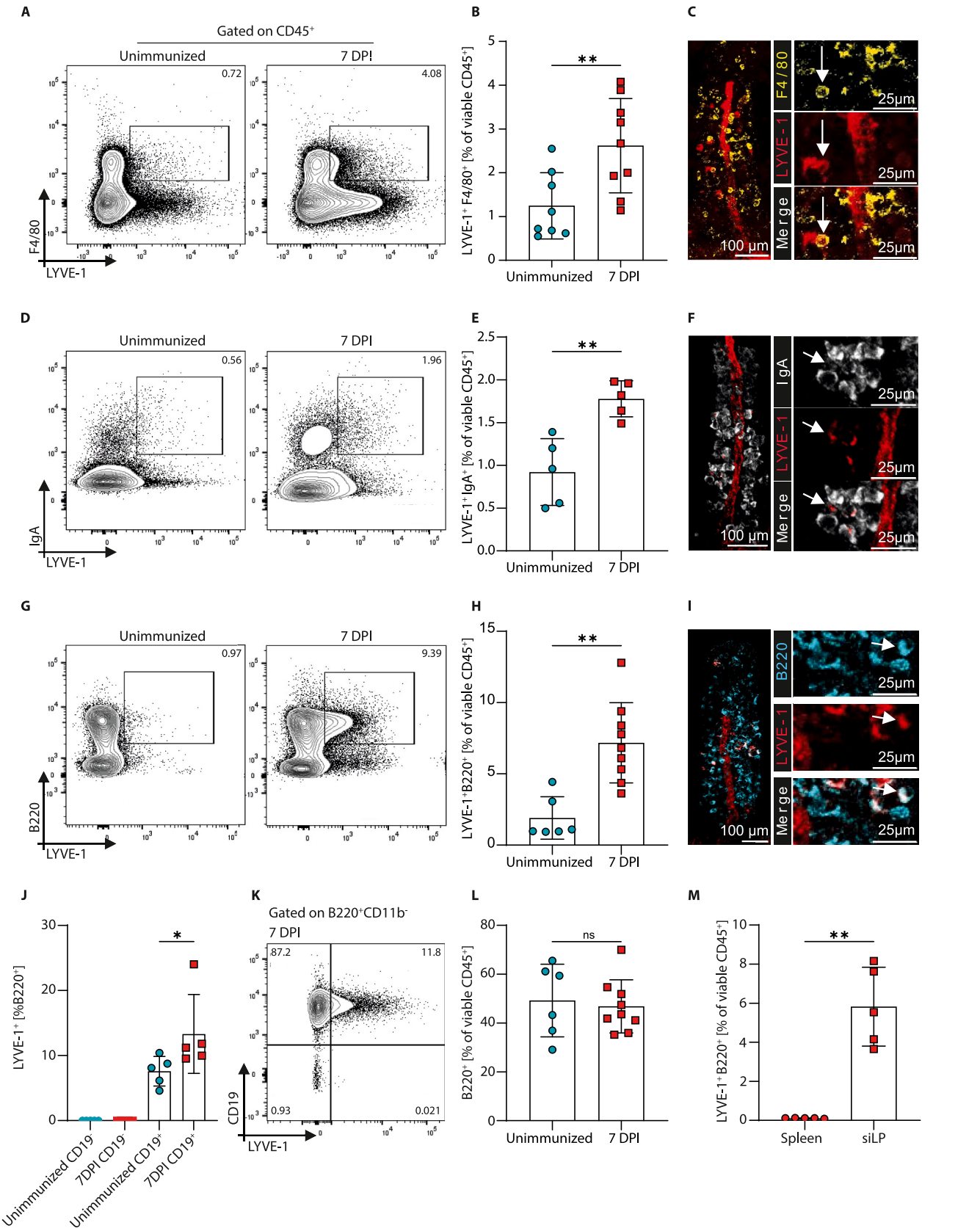

(caption on next page)

Fig. 4. Expansion of perivascular LYVE-1$^+$ is gut-specific and predominantly driven by LYVE-1$^+$ B cells. **(A–C)** Flow cytometry (n = 8–9 mice per group) and immunofluorescent analysis (n = 3 mice per group) of LYVE-1$^+$ macrophages with **(A)** representatives FACS plots, gated on viable CD45$^+$, for LYVE-1$^+$ and F4/80$^+$ co-expression in unimmunized mice (left panel) and mice immunized for EAE at 7 DPI (right panel) and **(B)** Quantification of LYVE-1$^+$ F4/80$^+$ cell frequency as gated in (A). **(C)** Representative whole-mount images stained for LYVE-1 (red) and F4/80 (yellow). Arrow indicates cell co-expressing LYVE-1 and F4/80. Scale bars represent 100 μm (left panel) or 25 μm (right panels). **(D–F)** Flow cytometry (n = 5 mice per group) and whole-mount immunostaining (n = 3 mice per group) of LYVE-1$^+$ IgA-expressing cells. **(D)** Illustrative FACS plot, gated on CD45$^+$ cells, for co-expression of IgA and LYVE-1, and **(E)** quantification of IgA$^+$ LYVE–1$^+$ during steady-state or in mice immunized for EAE at 7 DPI **(F)** Representative whole-mount immunostaining image for co-localization of LYVE-1 (red) and IgA (white). Arrow indicates cell stained for IgA and LYVE-1. Scale bars represent 100 μm (left panel) or 25 μm (right panels). **(G–I)** Flow cytometry (n = 6–9 mice per group) and immunofluorescent analysis (n = 3 per group) of LYVE-1$^+$ B cells. **(G)** Representative FACS plots were gated on viable CD45$^+$ for LYVE-1$^+$ and B220$^+$ co-expression in unimmunized mice (left panel) and mice immunized for EAE at 7 DPI (right panel). **(H)** Quantification of LYVE-1$^+$ B220$^+$ cell frequency as gated in (G). **(I)** Representative whole-mount images stained for LYVE-1 (red) and B220 (cyan). Arrow indicates cell co-expressing LYVE-1 and B220. Scale bars represent 100 μm (left panel) or 25 μm (right panels). **(J–K)** Evaluation of LYVE-1 expression among B220$^+$CD19$^+$ and B220$^+$CD19$^-$ cells by flow cytometry. **(J)** Quantification of B220$^+$CD19$^-$LYVE-1$^+$ and B220$^+$CD19$^+$LYVE-1$^+$ cell frequency among B220-expressing cells, and **(K)** representative FACS plot of LYVE-1 and CD19 co-expression in siLP from mice immunized for EAE at 7 DPI. **(L)** Flow cytometry analysis of total B220$^+$ cell frequency in siLP of mice immunized for EAE at 7 DPI. **(M)** Flow cytometry analysis of LYVE-1$^+$ B220$^+$ cell frequency in spleen and siLP of mice immunized for EAE at 7 DPI. Data from two experiments (B, H and L) or one experiment (E, J, and M), and representative of two (E, J) or three (B, H, L, M) independent experiments. Symbols represent biological replicates (B–M). Mean ± SD. ns: not significant, *P ≤ 0.05 and **P ≤ 0.01. Data were analyzed by two-tailed Mann-Whitney test (B–M).

the gut during autoimmunity.

3.5. LYVE-1$^+$ B cells are enriched for IgA and proangiogenic-related genes

We observed that LYVE-1$^+$ B cells represent the dominant population expanded after MOG/CFA/PTX immunization among CD45$^+$LYVE-1$^+$ immune cells (Fig. 3I). To identify transcriptional signatures and molecular pathways specific to LYVE-1$^+$ B cells, we sorted LYVE-1$^+$ and LYVE-1$^-$ B cells from the siLP at 7 DPI mice as viable CD45$^+$B220$^+$CD11b$^-$CD11c$^-$LYVE-1$^+$ and LYVE-1$^-$, respectively. RNA was extracted and paired bulk transcriptomic analysis of LYVE-1$^+$ and LYVE-1$^-$ B cells was performed. Using principal component analysis (PCA), we observed a distinctive transcriptomic signature between the two B cell subsets (Fig. 5A). Gene set enrichment analysis (GSEA) showed that LYVE-1$^-$ B cells transcriptome was mainly associated with inflammatory response, activation of the immune response or positive regulation of cytokine production (Fig. 5B). In contrast, LYVE-1$^+$ B cells were enriched in transcripts involved in oxidative phosphorylation, MTORC1 signaling, and cell cycle-related genes suggesting metabolic reprogramming and cell growth signaling (Fig. 5C). Consistent with the GSEA, LYVE-1$^-$ B cells featured a significantly enhanced expression of the pro-inflammatory chemokine *CCL5*, the growth factor granulocyte-macrophage colony-stimulating factor (GM-CSF, encoded by *Csf2* gene), as well as cytokines (*interferon-γ* and *Il17f*) and the co-stimulatory molecule 4-1BB (encoded by *TNFRSF9* gene) (Fig. 5D and E). This suggests that LYVE-1$^-$ B cells promote intestinal inflammation and immune cell recruitment previously described during presymptomatic EAE [36,67].

Lyve1 was the most differentially expressed gene between LYVE-1$^+$ versus LYVE-1$^-$ B cells (Fig. 5D). Furthermore, metabolic adaptations such as increased oxidative phosphorylation and MTORC1 signaling, observed in LYVE-1$^+$ B cells, are associated with differentiation of B lymphocytes in plasmablasts [89–91]. Those observations are in accordance with the significantly increased intestinal IgA$^+$LYVE-1$^+$ population identified above (Fig. 3H). We thus specifically tested the enrichment of transcripts related to IgA plasmablast and B cells terminal differentiation [92]. Indeed, we found that the transcription factor B-lymphocyte-induced maturation protein 1 (*Blimp-1*), the enzyme Activation-induced cytidine deaminase (*Aicda)*, involved in somatic hypermutation and class-switch recombination, IgA heavy chain (*Igha*) and *Jchain* (peptide required for IgA dimerization) were over-represented in LYVE-1$^+$ B cells (Fig. 5D and E). We further observed increased levels of hypoxia-inducible factor 1-alpha (*Hif1a*), the endothelial growth factor vascular endothelial growth factor B (*Vegfb*) and genes related to proliferation such as the proliferation marker protein Ki-67 (*Mki67*) and G2/mitotic-specific cyclin-B1 (*CCNB1*) in perivascular LYVE-1$^+$ B cells (Fig. 5D and E) [93,94]. We identified two genes of interest that were significantly enriched in LYVE-1$^+$ B cells: the high–mobility group box 1 (*Hmgb1*) and CD73 (*Nt5e*), associated with proangiogenic properties specifically in B cells [95,96]. CD73 is particularly interesting when considering the recent description of the proangiogenic B cell subset characterized by CD49b and CD73 expression that are significantly increased in melanoma and eosinophilic esophagitis in humans [96]. Furthermore, studies demonstrated that CD73 promotes angiogenesis in several cancer types and that its inhibition mitigates tumor neovascularization [73,97–99]. Therefore, we assessed CD73 protein expression level by flow cytometry in both LYVE-1 negative and positive B cell subsets at steady-state and after immunization for EAE (Fig. 5F). LYVE-1$^+$ B cells displayed a significantly higher expression level of CD73 compared to LYVE-1$^-$ B cells at the basal level. After EAE induction, CD73 expression was further upregulated in LYVE-1$^+$ B cells and, to a lesser extent, in LYVE–1$^-$ B cells. CD73 protein expression remained significantly reduced in LYVE-1$^-$ B cells during preclinical EAE compared to LYVE-1$^+$ B cells. Our results suggest that intestinal LYVE-1 positive B cells acquire a proangiogenic profile, proliferate and differentiate into IgA plasmablasts after immunization.

LYVE-1$^+$ B cells further display a phenotype enriched in markers associated with memory B cells to a greater extent than LYVE-1$^-$ B cells (Fig. S3). Flow cytometry analysis revealed higher CD27 expression level in LYVE-1$^+$ B cells compared to LYVE-1$^-$ B cells at steady state and at 7 DPI (Fig. S3A). The expression level of IgA was also significantly increased in the population of LYVE-1$^+$ IgA$^+$ cells compared to LYVE-1$^-$ IgA$^+$ cells (Fig. S3B). We compared the expression of surface markers associated with mouse naïve and memory B cells recently defined by Weisel et al. among LYVE-1$^-$ and LYVE-1$^+$ B cells obtained from our transcriptome analysis [100]. We observed enrichment in memory B cell-associated markers in LYVE-1$^+$ B cell, while LYVE-1$^-$ B cell displayed higher expression in naïve B cell-associated genes (Fig. S3C).

As inflammation can promote angiogenesis, we then asked whether intestinal barrier breakdown impacted the proangiogenic properties of LYVE-1$^+$ B cells following EAE induction [101]. To address this, we treated mice with larazotide acetate peptide (LA), a zonulin receptor antagonist proposed as a treatment for celiac disease [102]. LA specifically targets impaired intestinal barrier functions and efficiently reduces intestinal inflammation in an experimental model of IBD [103]. We thus treated unimmunized and mice immunized for EAE orally with LA to restore intestinal barrier integrity and assessed the expansion and phenotype of intestinal LYVE-1$^+$ B cells. We extracted immune cells from the jejunum of mice receiving pharmacological or sham treatments at steady state and at 7 DPI (Fig. 5G). We did not observe an effect of LA treatment on the expansion of LYVE-1$^+$ B cells during preclinical EAE. The expression level of CD73 in LYVE-1$^+$ B cells isolated from unimmunized mice was not impacted by LA treatment (Fig. 5H), but was significantly reduced in immunized mice receiving LA compared to

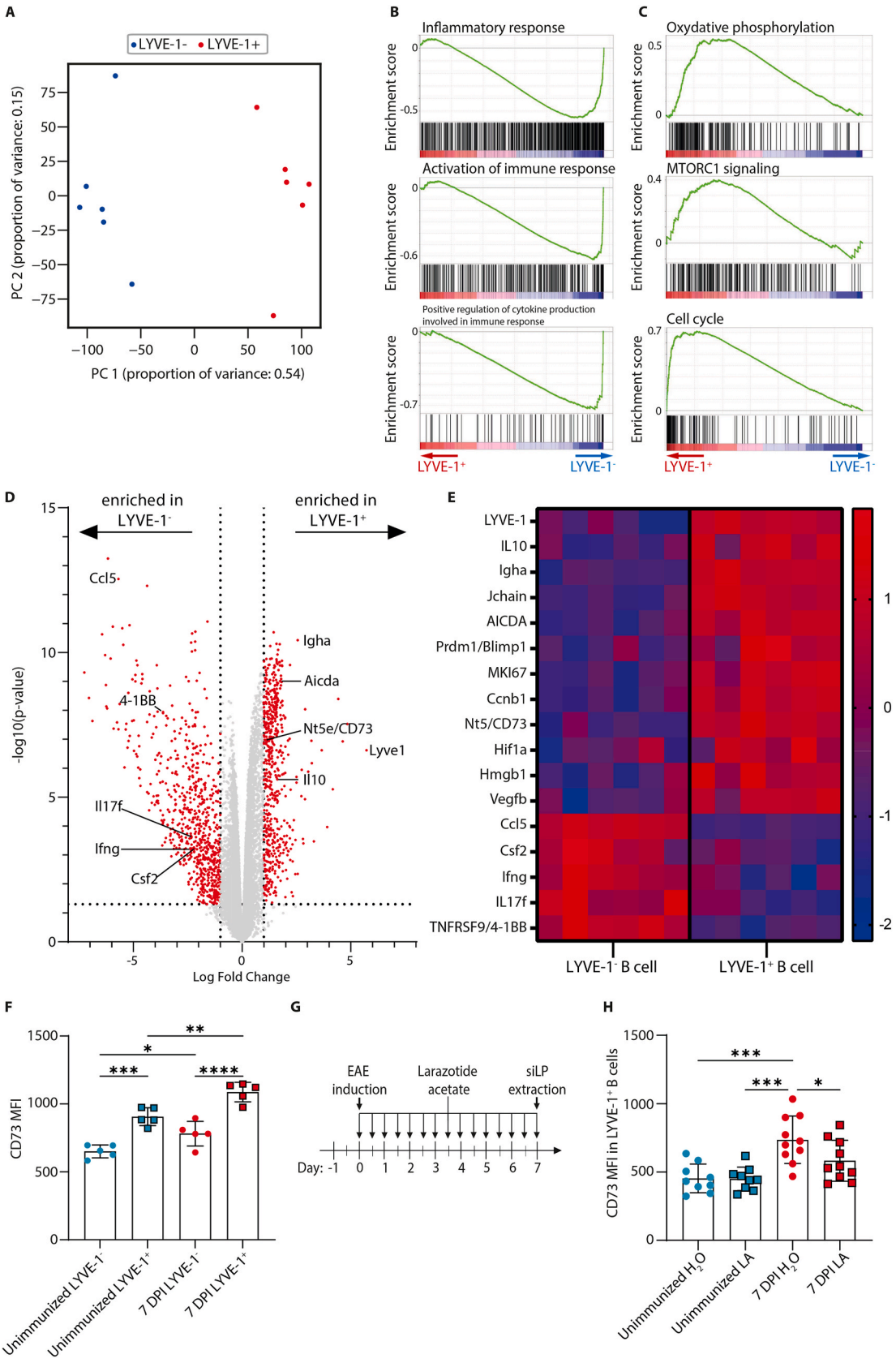

(caption on next page)

Fig. 5. LYVE-1$^+$ B cell transcriptome reveals proliferative and proangiogenic potential. **(A)** PCA was performed on the transcriptomic signature of LYVE-1$^+$ B cell (red dots) and LYVE-1- B cell (blue dots) isolated from siLP of 6 mice immunized for EAE at 7 DPI. **(B)** GSEA of LYVE-1$^-$ B cells transcriptome (n = 6 mice) shows enrichment in gene related to inflammatory response (top panel, NES = −1.8, False discovery rate [FDR] = 0.0), activation of immune response (middle panel, NES = −1.98, FDR = 0.002) and positive regulation of cytokine production involved in immune response (bottom panel, NES = −1.92, FDR = 0.002) compared to LYVE-1$^+$ B cells. **(C)** GSEA of LYVE-1$^+$ B cell transcriptome of mice immunized for EAE at 7 DPI (n = 6 mice) demonstrates an enrichment in genes related to oxidative phosphorylation (top panel, NES = 2.18, FDR = 0.0), MTORC1 signaling (middle panel, NES = 1.34, FDR = 0.0) and cell cycle (bottom panel, NES = 1.92, FDR = 0.0) compared to LYVE$^-$ B cells. **(D)** Volcano plot showing differential gene expression between LYVE-1$^+$ and LYVE-1$^-$ B cells with $p < 0.05$ and fold change >2. **(E)** Heatmap showing normalized expression (z-score) of selected gene count from transcriptomic analysis. **(F)** Expression level of CD73 in the indicated B cell populations (n = 5 mice per group) extracted from the siLP of unimmunized (blue) and mice immunized for EAE at 7 DPI (red) depending on their expression of LYVE-1. CD73 expression level was assessed by flow cytometry and bars represent the geometric mean fluorescence intensity (MFI) of CD73 staining. **(G)** Experimental design of larazotide acetate (LA) treatment by oral gavage following EAE induction. **(H)** Expression level of CD73 among LYVE-1 positive B cells contained in siLP following larazotide acetate or sham (H_2O) treatment, as presented in (G) at steady-state or in mice immunized for EAE at 7 DPI (n = 9–10 mice per group). CD73 expression level was assessed by flow cytometry and bars represent the geometric mean fluorescence intensity (MFI) of CD73 staining. Data from one experiment (A to F), representative of two independent experiments (F) or were combined from two independent experiments with similar results (H). Symbols represent biological (F and H) replicates. Mean ± SD. *P ≤ 0.05, **P ≤ 0.01 and ***P ≤ 0.001. Data were analyzed by ordinary one-way ANOVA with Tukey's multiple comparisons test (F) or Dunnett's multiple comparisons test (H).

water, reaching a similar level to mice at steady-state (Fig. 5H). Together, these results suggest that CD73 is upregulated in LYVE-1$^+$ B cells in response to increased intestinal permeability after EAE induction.

3.6. LYVE-1$^+$ B cells have proangiogenic properties

Based on the specific enrichment of proangiogenic markers in LYVE-1$^+$ B cell population isolated from EAE-induced mice, we hypothesized that intestinal LYVE-1$^+$ but not LYVE-1$^-$ B cells promote angiogenesis that we initially observed in the intestine. We used an adapted version of the aortic ring assay to investigate the proangiogenic role of the LYVE-1$^+$ B cells *in vitro* [53,54]. Aortic rings were stimulated for 3 days with basic fibroblast growth factor (bFGF) to promote endothelial cell growth. After 3 days, growth factor-containing media was removed, and fresh medium containing FACS-sorted intestinal LYVE-1$^+$ or LYVE-1$^-$ B cells from mice immunized for EAE at 7 DPI was added. We used media alone or media complemented with bFGF as negative and positive controls, respectively, and checked that the aortic sprouting area was similar in all conditions tested before sorted B cells were added (Fig. 6A quantification and illustrative images). Following 5 days of co-cultures, we observed a significantly increased aortic sprouting area in the presence of LYVE-1$^+$ B cells compared to LYVE-1$^-$ B cells co-cultures and negative control (Fig. 6B quantification and representative images). To evaluate LYVE-1$^+$ B cells location, we stained LYVE-1$^+$ B cells and LYVE-1$^-$ B cells after cell sorting separately with CFSE before co-culture with aortic rings. CFSE-labeled LYVE-1$^+$ B cells migrate close to sprouting endothelial cells and formed small aggregates in close vicinity of the vessel (Fig. 6C), which is reminiscent of their *in vivo* localization. LYVE-1$^-$ B cells were not observed close to sprouting endothelial cells.

To further confirm the involvement of intestinal B cells and no other cell types, including macrophages, in intestinal angiogenesis observed *in vivo* in mice immunized for EAE, we depleted B cells with a monoclonal anti-CD20 antibody or isotype control 7 days before EAE. siLP was extracted at 7 DPI to assess the consequences of B cell depletion on endothelial compartments in siLP (Fig. 6D). We first confirmed that anti-CD20 antibody treatment efficiently depleted B220$^+$ CD19$^+$ B cells in the small intestine, blood, spleen and mesenteric lymph nodes (Fig. 6E and representative FACS plot Fig. S4A), including intestinal LYVE-1$^+$ B cells compared to control mice (Figs. S4B–C). Depletion of intestinal B cells significantly decreased total BEC frequency in mice immunized for EAE, but not in unimmunized control mice (Fig. 6F). Furthermore, PLVAP-expressing BECs were significantly decreased in mice immunized for EAE following anti-CD20 treatment compared to immunized mice injected with isotype control (Fig. 6G). B cell depletion in immunized mice could not completely revert BEC and PLVAP$^+$ BEC expansion. This indicates that while B cells participate in intestinal angiogenesis, they are not the sole players in destabilization of the GVB. These results indicate that intestinal LYVE-1$^+$ B cells possess proangiogenic properties *in vitro* and that depletion of total B cells *in vivo* is sufficient to significantly decrease the abundance of LYVE-1$^+$ B cells, leading to the reduction of siLP BEC and BEC-expressing vascular permeability marker. Therefore, we propose that LYVE-1$^+$ B cells initiate intestinal vascular remodeling and expansion during early stages of EAE.

4. Discussion

Great emphasis has been recently placed on the alteration of the GVB in multiple animal models, including liver disease, colorectal cancer, and intestinal inflammatory diseases. However, investigations regarding its involvement during autoimmune disorders and CNS inflammatory diseases are lacking [104–106]. In this study, we describe small intestinal microvasculature remodeling in mice immunized for EAE prior to neurological symptoms onset highlighted by an increase of intestinal capillary diameter, an expansion of BEC numbers and an increased expression of the vascular permeability marker PLVAP. Concomitantly, we observed an elevation of intestinal vascular permeability in immunized mice. We further identify a subset of intestinal B cells expressing the surface marker LYVE-1 that promote intestinal angiogenesis and perturb GVB. Altogether, our results strengthen the contribution of the gut-brain axis during neuroinflammation and suggest a role for B cells in intestinal angiogenesis.

We show that immunization with CFA is the main driver of our observations that are not MOG_{35-55}-specific. As we observe similar changes in intestinal angiogenesis and LYVE-1$^+$ B cell expansion in mice immunized with PBS/CFA compared to MOG/CFA immunized mice. Nevertheless this is relevant to EAE as CFA is required to induce active EAE in mice. Previous studies have demonstrated that immunization with MOG_{35-55} emulsified in incomplete Freund's adjuvant (IFA, lacking *Mycobacteria*) is inefficient at inducing EAE [107]. However, complementation of MOG/IFA immunization with Toll-like Receptor agonists, such as LPS and, to a lesser extent, Zymosan or Poly I:C, restores development of EAE in MOG/IFA-immunized mice [108]. Additional data indicate that the presence of microbial-derived molecules such as peptidoglycan can act as sufficient adjuvant when mice are immunized with MOG/IFA [109]. The alteration of intestinal barrier integrity observed in CFA-immunized mice and subsequent dissemination of microbial-derived molecules might represent a necessary parameter for the loss of self-tolerance towards a give antigen, MOG_{35-55} in the case of EAE. CFA is used in multiple protocols of experimental autoimmunity, including experimental autoimmune myocarditis and collagen-induced arthritis [110,111]. Interestingly, intestinal barrier dysfunctions are reported to participate to disease pathogenesis in those models [112,113]. Our results thus suggest that changes in the GVB and in pro-angiogenic LYVE-1$^+$ B cells observed in the small intestine are not solely restricted to central nervous system inflammation and could contribute not only to neuroinflammation but also to other autoimmune diseases in particular when the gut compartment is implicated.

Figure 6

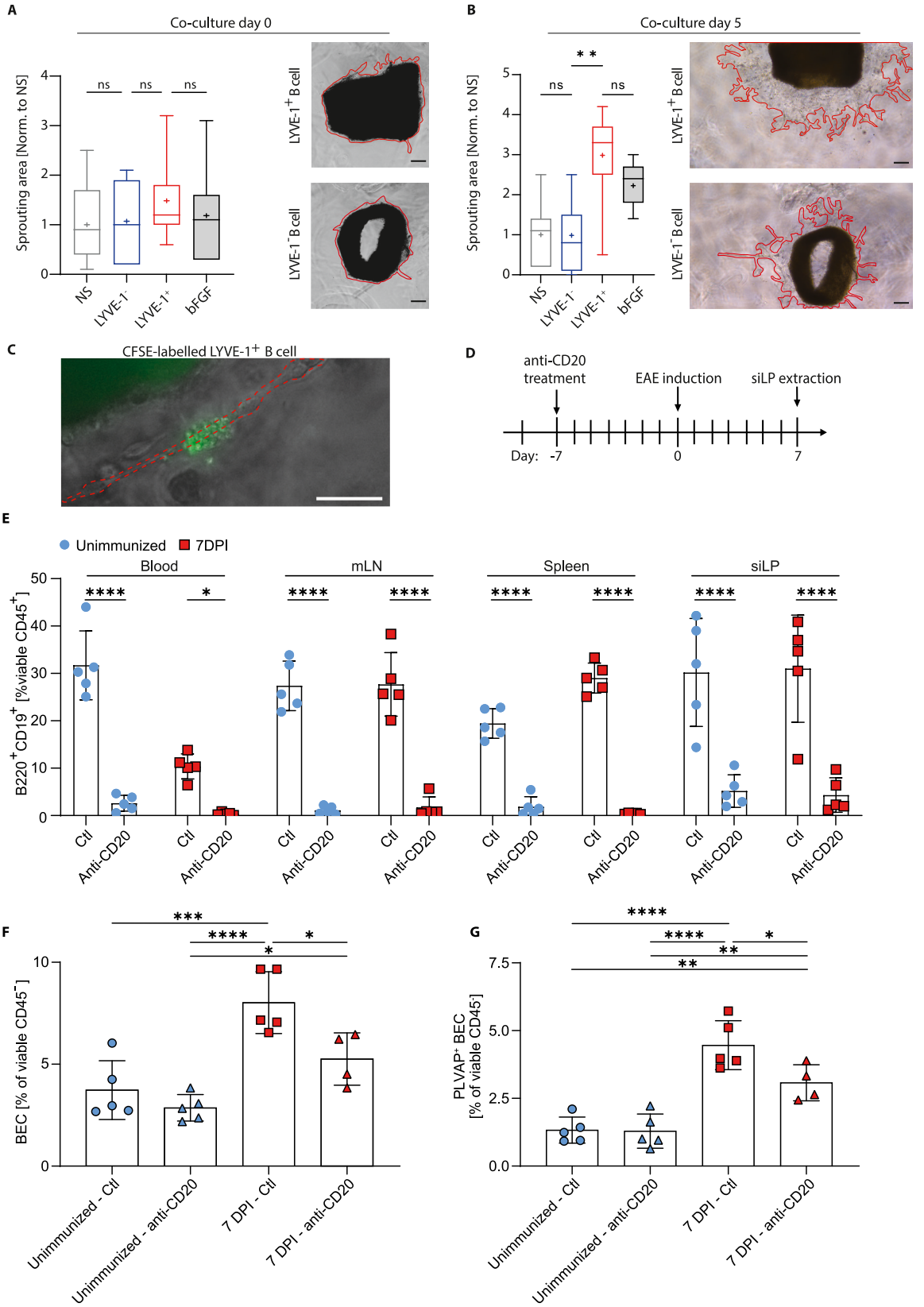

(caption on next page)

Fig. 6. Small intestinal LYVE-1$^+$ B cells exhibit proangiogenic activity. **(A)** Quantification of the sprouting area (left panel) during aortic ring assay prior to co-culture with LYVE-1$^-$ or LYVE-1$^+$ B cells isolated from siLP of mice immunized for EAE and representative images (right panels). NS: non-stimulated, LYVE-1$^-$: co-culture of aortic ring with sorted LYVE-1$^-$ B cell, LYVE-1$^+$: co-culture of aortic ring with sorted LYVE-1$^+$ B cell, bFGF: Aortic ring stimulated with 20 ng/ml basic fibroblast growth factor (bFGF) (n = 7 per group, siLP LYVE-1$^-$ and LYVE-1$^+$ B cell isolated from 5 mice immunized for EAE at 7 DPI). Results are normalized to the mean sprouting area measured in NS condition. Scale bars represent 200 μm. **(B)** Quantification of the sprouting area (left panel) during aortic ring assay following 5 days of co-culture with FACS-sorted LYVE-1$^-$ and LYVE-1$^+$ B cells and representative images (right panels). Results are normalized to the mean sprouting area measured in NS condition at the same time point. Scale bars represent 200 μm. **(C)** Representative image of CFSE-labeled LYVE-1$^+$ B cells migrating close to sprouting endothelial cells during aortic ring co-culture assay. Red line outline sprouting endothelial cells. Scale bar represent 50 μm. **(D)** Experimental design for anti-CD20 or isotype control antibody treatment prior to EAE induction. **(E)** Quantification of B cell frequency determined by flow cytometry (CD19$^+$B220$^+$) among viable CD45$^+$ cells in blood, mesenteric lymph nodes (mLN), spleen and siLP (duodenum) of unimmunized controls (blue circles) and mice immunized for EAE at 7 DPI (red squares) following treatment with anti-CD20 antibody (anti-CD20) or isotype control antibody (Ctl) (n = 5 mice per group). **(F)** Quantification of BEC (CD45$^-$CD31$^+$ podoplanin$^-$) frequency isolated from siLP (jejunum) of unimmunized controls (blue) and mice immunized for EAE at 7 DPI (red) following anti-CD20 antibody (triangles) or isotype control treatment (circles). **(G)** Quantification of PLVAP$^+$ BECs frequency in siLP of unimmunized controls (blue) and mice immunized for EAE at 7 DPI (red) following anti-CD20 antibody (triangles) or isotype control treatment (circles) determined by flow cytometry. Data representative of two independent experiments (A–G). Symbols represent biological (E–G) replicates. Mean ± SD. *P ≤ 0.05, **P ≤ 0.01, ***P ≤ 0.001 and ****P < 0.0001. Data were analyzed by ordinary one-way ANOVA with Holm-Šídák's multiple comparisons test (A, B, F and G) or two-way ANOVA with Šídák's multiple comparisons test (E).

Upregulation of BEC proliferation-associated genes cyclin D3, a key regulator of the transition from G1 to S phase during the cell cycle, and the transforming growth factor β (TGFβ) superfamily co-receptor endoglin observed in BEC at 7 DPI further support the ongoing proliferation of intestinal vasculature [114,115]. Endoglin expression is linked to vascular remodeling, and its upregulation has been observed in tissues undergoing active angiogenesis [116]. Interestingly, a soluble form of endoglin is increased in the serum of pwMS, together with other angiogenic factors [117]. Antiangiogenic treatments during EAE have shown to be beneficial. Treatment targeting VEGF signaling (i.e., bevacizumab) during EAE reduces disease severity and attenuates demyelination when started at EAE clinical onset [118]. However, data regarding antiangiogenic treatment during the preclinical phase of EAE are lacking. Our results suggest that antiangiogenic treatment during the presymptomatic phase of EAE could enhance its efficacy by promoting GVB integrity.

A majority of proangiogenic growth factors initiate their action by promoting vascular permeability. Angiogenesis is associated with increased vascular leakage, particularly in pathological conditions [119,120]. The observation of elevated serum LPS (50–100 kDa) in pwMS and mice with EAE, as well as translocation of FITC-coupled BSA (66 kDa), can be seen as circumstantial evidence of GVB injury, which fails to limit macromolecule entry, including microbial-derived pro-inflammatory molecules [8,36,39]. Here, we report an upregulation of PLVAP protein on siLP BEC and increased extravasation of Evans blue dye in the small intestine after immunization, indicating that angiogenesis is concomitant with excessive vessel permeability. While it is unclear whether gut-derived pro-inflammatory molecules already enter the systemic circulation at 7 DPI, dysbiosis and elevation of the marker of intestinal inflammation calprotectin are apparent at this early time point [37,121]. Interestingly, calprotectin activates endothelial cells and increases monolayer permeability *in vitro* [122]. While the impact of intestinal angiogenesis on GVB function is poorly characterized, intestinal BECs highly upregulate angiogenesis-related genes upon *Salmonella typhimurium* infection, which provokes GVB injury [43]. Furthermore, concomitant intestinal angiogenesis and increased intestinal BEC permeability was shown *in vivo* using the DSS-induced colitis model or *Clostridium difficile* infection and *in vitro* culture of rat intestinal microvascular endothelial cells [52,123,124]. Together, those observations indicate that intestinal endothelial cell proliferation, inflammation, and breach of the vascular barrier are concomitant and likely related to each other. It is conceivable that excessive intestinal epithelial barrier permeability and low-grade microbial translocation induce immune cell recruitment and activation, generating a hypoxic environment. This is supported by the high expression level of the Hypoxia-inducible Factors 1-alpha (*Hif1a*) transcription factor observed among LYVE-1$^+$ and LYVE-1$^-$ B cells during transcriptomic analysis. While *Hif1a* expression was enriched in LYVE-1$^+$ B cells, being in the top 5 % of the most expressed gene based on our transcriptomic analysis, its expression among LYVE-1$^-$ B cells was found in the top 10 % gene with the highest expression level, suggestive of intestinal hypoxia. We thus propose that intestinal angiogenesis, promoted by hypoxia and inflammation, destabilizes the GVB structure, reducing its capacity to maintain proper vascular permeability. In turn, systemic dissemination of gut-derived pro-inflammatory molecules might promote bystander activation and/or molecular mimicry on autoreactive immune cells and alter BBB permeability, thus participating in CNS autoimmunity.

We propose that one driver of intestinal angiogenesis are perivascular LYVE-1-expressing B cells. LYVE-1 is a hyaluronic acid (HA) receptor whose expression has been reported in lymphatic vessels and subsets of tissues resident macrophages, blood sinusoidal endothelial cells in the liver and the spleen, as well as non-sinusoidal endothelial cell in the heart, lungs, and adrenal glands [125–127]. HA is a major component of the extracellular matrix. When transfected into 293T fibroblasts *in vitro*, LYVE-1 mediates the internalization of HA, and has thus been proposed to participate in HA tissue clearance and catabolism [128]. Furthermore, LYVE-1 is required for efficient DC lymphatic trafficking from inflamed skin to draining lymph nodes [129]. DCs (and other leukocytes) produce HA as a constituent of the cell glycocalyx [129,130]. Engagement of LYVE-1 with HA-coat promotes docking of DCs on lymphatics and their subsequent transmigration, an interaction that can be exploited by HA-encapsulated pathogens, such as Group A streptococcus, to facilitate bacteria dissemination [129,131]. HA displays dichotomous biological functions depending on its molecular weight. Under homeostatic conditions, HA forms polymeric molecules called high molecular weight (HMW) HA of up to several million Daltons [132]. During inflammation, HA accumulates in tissue, and its degradation by hyaluronidases and reactive oxygen species produces low molecular weight (LMW) HA [133–135]. HMW HA exhibits anti-inflammatory properties, inhibits EC proliferation, and disturbs EC monolayer *in vitro*, indicating antiangiogenic and regulatory effects [136,137]. Conversely, LMW HA is proinflammatory and promotes EC proliferation and migration *in vitro* and angiogenesis *in vivo* [138–142]. In the intestine, HMW HA has been shown to stimulate intestinal epithelial cell proliferation, while inhibiting HA's binding with its receptors has the opposite effect [143]. Intestinal HA is increased in the LP during DSS-induced colitis and is found elevated in inflamed compared to noninflamed colon tissues of IBD patients [133,144]. Moreover, exogenous hyaluronan administration is beneficial in a TLR-4-dependent manner in DSS-induced colitis [144]. Additionaly, inhibition of HA sythesis is protective in the context of EAE [145]. Further investigations are warranted to ascertain whether intestinal HA metabolism is altered following EAE immunization, with the potential involvement of LYVE-1$^+$ immune cells.

The role of B cells in MS is well established and B cell depletion is a pivotal treatment of this disease as well as other systemic autoimmune disorders [146,147]. Multiple underlying mechanisms of B cells in promoting autoimmunity have been unraveled. We here propose a novel

function of B cells in driving angiogenesis in the gut and disrupting the GVB. Expression of LYVE-1 was described in different immune cell subsets. LYVE-1$^+$ macrophages with proangiogenic properties were identified in adipose tissues, dental pulp, and tumor microenvironment and display a similar phenotype in the intestine during inflammation [81–83]. Moreover, LYVE-1$^+$ macrophages have the ability to degrade collagen content in vascular smooth muscle cells (SMCs), which requires the engagement of LYVE-1 with HA on SMCs [148]. Regarding LYVE-1 expression among B cells, Takeda et al. demonstrated using Lyve1-CRE/R26-tdTomato reporter mice that a considerable proportion of lymph node and splenic B cells, as well as thymocytes, express *Lyve1* [149]. However, leukocytes from this *Lyve1*$^+$ lineage did not display cell surface expression of LYVE-1 protein, consistent with our data on splenic B cells during EAE [149]. The function of LYVE-1 in B cells is yet unexplored and opens new area of research. CD44 is the closest homologue of LYVE-1 [125]. In B cell, CD44-HA interaction promotes proliferation, differentiation, chemotaxis and secretion of anti-inflammatory cytokines [150,151]. Furthermore, HA stimulation enhances wound repair potential of B cells through TLR4 in a CD19-dependent manner [152]. Inflammatory stimuli induce upregulation of HA synthesis in EC *in vitro*, increasing monocyte adhesion through HA-CD44 interaction [153]. LYVE-1 might similarly promote B cell adhesion to blood EC, potentially supporting paracrine signaling between EC and proangiogenic B cells.

Our transcriptomic and flow cytometric experiments on LYVE-1$^+$ B cells reveal a proliferating phenotype expressing high levels of the ecto-5′-nucleotidase CD73. CD73 acts in concert with CD39 (detected in LYVE-1$^-$ and LYVE-1$^+$ B cells in our transcriptomic analysis) to generate adenosine from extracellular ATP [154]. Previous studies demonstrate that adenosine has a proangiogenic effect *in vitro* by promoting endothelial cell proliferation and migration and enhancing angiogenesis *in vivo* [155,156]. In addition, targeting CD73 in a mouse model of breast cancer abrogates tumor angiogenesis *in vivo* [157]. How CD73 expression is regulated in B cells is unclear, however its expression is induced by hypoxia and inflammation in endothelial cells, T cells, and tumor cells [158–160]. Interestingly, a recent report has identified a proangiogenic B cell subset characterized by surface expression of CD49b and CD73, whose frequency was increased during chronic inflammation and melanoma patients [96]. However, contradictory accounts exist regarding implication of CD73 expression during EAE. While one study reported a reduced immune cell infiltration in CNS and severity of EAE in CD73$^{-/-}$ mice, an independent report observed no effect of CD73 deficiency on EAE pathogenesis [161,162]. The proliferative phenotype of LYVE-1$^+$ B cells is also of interest when considering the recent identification of proliferative peritumoral B cells driving proangiogenic response in a tumor-derived HMGB1-dependant manner, which we found increased in LYVE-1$^+$ B cell transcriptome [95]. We demonstrate here the proangiogenic potential of gut-derived LYVE-1$^+$ B cells *in vitro* using an aortic ring assay co-culture where LYVE-1$^+$ B cells were able to promote endothelial cell sprouting to a greater extent than their LYVE-1$^-$ B cells counterpart. Furthermore, B cell depletion decreases the absolute number of intestinal LYVE-1$^+$ B cells, siLP BEC, and reduces the expression of PLVAP in BEC. Our results are in accordance with a recent publication showing that B cell depletion during EAE improves BBB integrity and reduces blood vessel dilation by promoting the expression of gene pathways involved in neurovascular coupling from astrocytes [163]. This further suggests a pivotal role of B cells in the maintenance of vascular integrity during neuroinflammation.

Altogether, our results demonstrate that B cells support intestinal BEC proliferation and promote alteration of vascular permeability following EAE immunization. Our data indicate an expansion of proangiogenic perivascular B cells characterized by LYVE-1 expression displaying an overlapping phenotype with proangiogenic B cells recently described in human pathologies, including during chronic inflammation. While we demonstrate the proangiogenic properties of LYVE-1$^+$ B cells *in vitro* and *in vivo*, the underlying mechanism however remains to be determined that we could not address here. In particular, CD73 inhibition during presymptomatic EAE and its effect on intestinal angiogenesis should be investigated. This approach would, however, have its own pitfalls as CD73-derived adenosine also has immunoregulatory properties [164]. Thus, CD73 blockade would simultaneously inhibit angiogenesis and exacerbate inflammation, thus challenging the result interpretation. As we depleted the whole B cell population, and not specifically the LYVE-1$^+$ B cell, we cannot exclude that LYVE-1$^-$ B cells, which did not promote angiogenesis in the aortic ring assay, indirectly impact the vascular compartment. Furthermore, other cell types composing the GVB, namely enteric glial cells and pericytes, or LYVE-1$^+$ macrophages, could be affected during EAE. Finally, it is possible that LYVE-1$^+$ immune cell expansion and angiogenesis are shared with other mucosal sites and are not restricted to the small intestine. Our results thus opens new avenues of research on interactions of immune cells and angiogenesis in mucosal tissues during autoimmunity.

In conclusion, we propose that the expansion of the vasculature in the small intestine induces GVB destabilization, potentially promoting systemic inflammation and potentially favoring tolerance breakdown. Targeting intestinal immune cell induced-angiogenesis could lead to promising approaches to target autoimmunity.

Funding

This work was supported by the Leenaards Foundation (to CP, TVP), the Swiss National Science Foundation (PP00P3-157476 to CP; 310030-192738 to CP; MD-PhD grant 323630-183987 to FR; CRSK-3_190435 to JBL), the Swiss MS Society («Research Grant No. 2021–13") (to CP), the Fondation Panacée (to CP) and the Muschamps Foundation (to JBL).

Data and materials availability

All data, code, and materials used in the analysis are available to any researcher for purposes of reproducing or extending the analysis. All data are available in the main text or the Supporting Information. RNA-seq data produced in this study have been submitted to Gene Expression Omnibus (GEO) and are available under the accession number GSE271603.

CRediT authorship contribution statement

Benjamin Peter: Conceptualization, Formal analysis, Investigation, Methodology, Visualization, Writing – original draft, Writing – review & editing. **Jessica Rebeaud:** Investigation, Writing – review & editing. **Solenne Vigne:** Conceptualization, Investigation, Methodology, Supervision, Writing – original draft, Writing – review & editing. **Valentine Bressoud:** Investigation, Writing – review & editing. **Nicholas Phillips:** Investigation, Writing – review & editing. **Florian Ruiz:** Investigation, Writing – review & editing. **Tatiana V. Petrova:** Writing – review & editing. **Jeremiah Bernier-Latmani:** Investigation, Writing – review & editing. **Caroline Pot:** Conceptualization, Funding acquisition, Methodology, Project administration, Supervision, Visualization, Writing – original draft, Writing – review & editing.

Declaration of competing interest

Authors declare that they have no competing interests.

Acknowledgments

We thank D. Duc and M. S. Iatrou for preliminary data generation. We would like to thank the Lausanne Genomic Technologies Facility for performing the RNA sequencing, the Flow Cytometry Facility of the Lausanne University for performing cell sorting experiments. The animal and Cellular Imaging Facilities of Lausanne University are gratefully acknowledged for their participation in this study.

Appendix A. Supplementary data

Supplementary data to this article can be found online at https://doi.org/10.1016/j.jaut.2024.103292.

References

[1] M.E.V. Johansson, J.K. Gustafsson, J. Holmén-Larsson, K.S. Jabbar, L. Xia, H. Xu, F.K. Ghishan, F.A. Carvalho, A.T. Gewirtz, H. Sjövall, G.C. Hansson, Bacteria penetrate the normally impenetrable inner colon mucus layer in both murine colitis models and patients with ulcerative colitis, Gut 63 (2014) 281–291, https://doi.org/10.1136/gutjnl-2012-303207.

[2] F. Ciccia, G. Guggino, A. Rizzo, R. Alessandro, M.M. Luchetti, S. Milling, L. Saieva, H. Cypers, T. Stampone, P. Di Benedetto, A. Gabrielli, A. Fasano, D. Elewaut, G. Triolo, Dysbiosis and zonulin upregulation alter gut epithelial and vascular barriers in patients with ankylosing spondylitis, Ann. Rheum. Dis. 76 (2017) 1123–1132, https://doi.org/10.1136/annrheumdis-2016-210000.

[3] R. Carratù, M. Secondulfo, L. De Magistris, D. Iafusco, A. Urio, M.G. Carbone, G. Pontoni, M. Cartenì, F. Prisco, Altered intestinal permeability to mannitol in diabetes mellitus type I, J. Pediatr. Gastroenterol. Nutr. 28 (1999) 264–269, https://doi.org/10.1002/j.1536-4801.1999.tb02061.x.

[4] D. Azzouz, A. Omarbekova, A. Heguy, D. Schwudke, N. Gisch, B.H. Rovin, R. Caricchio, J.P. Buyon, A.V. Alekseyenko, G.J. Silverman, Lupus nephritis is linked to disease-activity associated expansions and immunity to a gut commensal, Ann. Rheum. Dis. 78 (2019) 947–956, https://doi.org/10.1136/annrheumdis-2018-214856.

[5] D.E. Matei, M. Menon, D.G. Alber, A.M. Smith, B. Nedjat-Shokouhi, A. Fasano, L. Magill, A. Duhlin, S. Bitoun, A. Gleizes, S. Hacein-Bey-Abina, J.J. Manson, E. C. Rosser, N. Klein, P.A. Blair, C. Mauri, Intestinal barrier dysfunction plays an integral role in arthritis pathology and can be targeted to ameliorate disease, Med 2 (2021) 864–883.e9, https://doi.org/10.1016/j.medj.2021.04.013.

[6] R. Lin, L. Zhou, J. Zhang, B. Wang, Abnormal intestinal permeability and microbiota in patients with autoimmune hepatitis, Int. J. Clin. Exp. Pathol. 8 (2015) 5153–5160.

[7] F.L.A. Yusuf, F. Zhu, C. Evans, J.D. Fisk, Y. Zhao, R.A. Marrie, H. Tremlett, Gastrointestinal conditions in the multiple sclerosis prodrome, Ann Clin Transl Neurol 11 (2024) 185–193, https://doi.org/10.1002/acn3.51945.

[8] B.M. Escribano, F.J. Medina-Fernández, M. Aguilar-Luque, E. Agüera, M. Feijoo, F.I. Garcia-Maceira, R. Lillo, P. Vieyra-Reyes, A.I. Giraldo, E. Luque, R. Drucker-Colín, I. Túnez, Lipopolysaccharide binding protein and oxidative stress in a multiple sclerosis model, Neurotherapeutics 14 (2017) 199–211, https://doi.org/10.1007/s13311-016-0480-0.

[9] I. Cosorich, G. Dalla-Costa, C. Sorini, R. Ferrarese, M.J. Messina, J. Dolpady, E. Radice, A. Mariani, P.A. Testoni, F. Canducci, G. Comi, V. Martinelli, M. Falcone, High frequency of intestinal T_H 17 cells correlates with microbiota alterations and disease activity in multiple sclerosis, Sci. Adv. 3 (2017) e1700492, https://doi.org/10.1126/sciadv.1700492.

[10] S. Jangi, R. Gandhi, L.M. Cox, N. Li, F. Von Glehn, R. Yan, B. Patel, M.A. Mazzola, S. Liu, B.L. Glanz, S. Cook, S. Tankou, F. Stuart, K. Melo, P. Nejad, K. Smith, B. D. Topçuolu, J. Holden, P. Kivisäkk, T. Chitnis, P.L. De Jager, F.J. Quintana, G. K. Gerber, L. Bry, H.L. Weiner, Alterations of the human gut microbiome in multiple sclerosis, Nat. Commun. 7 (2016) 12015, https://doi.org/10.1038/ncomms12015.

[11] D. Takewaki, W. Suda, W. Sato, L. Takayasu, N. Kumar, K. Kimura, N. Kaga, T. Mizuno, S. Miyake, M. Hattori, T. Yamamura, Alterations of the gut ecological and functional microenvironment in different stages of multiple sclerosis, Proc. Natl. Acad. Sci. U.S.A. 117 (2020) 22402–22412, https://doi.org/10.1073/pnas.2011703117.

[12] K. Berer, L.A. Gerdes, E. Cekanaviciute, X. Jia, L. Xiao, Z. Xia, C. Liu, L. Klotz, U. Stauffer, S.E. Baranzini, T. Kümpfel, R. Hohlfeld, G. Krishnamoorthy, H. Wekerle, Gut microbiota from multiple sclerosis patients enables spontaneous autoimmune encephalomyelitis in mice, Proc. Natl. Acad. Sci. U.S.A. 114 (2017) 10719–10724, https://doi.org/10.1073/pnas.1711233114.

[13] M.C. Buscarinu, B. Cerasoli, V. Annibali, C. Policano, L. Lionetto, M. Capi, R. Mechelli, S. Romano, A. Fornasiero, G. Mattei, E. Piras, D.F. Angelini, L. Battistini, M. Simmaco, R. Umeton, M. Salvetti, G. Ristori, Altered intestinal permeability in patients with relapsing–remitting multiple sclerosis: a pilot study, Mult. Scler. 23 (2017) 442–446, https://doi.org/10.1177/1352458516652498.

[14] M.C. Buscarinu, F. Gargano, L. Lionetto, M. Capi, E. Morena, A. Fornasiero, R. Reniè, A.C. Landi, G. Pellicciari, C. Romano, R. Mechelli, S. Romano, G. Borsellino, L. Battistini, M. Simmaco, C. Fagnani, M. Salvetti, G. Ristori, Intestinal permeability and circulating CD161+CCR6+CD8+T cells in patients with relapsing–remitting multiple sclerosis treated with dimethylfumarate, Front. Neurol. 12 (2021) 683398, https://doi.org/10.3389/fneur.2021.683398.

[15] A. Mirza, Y. Mao-Draayer, The gut microbiome and microbial translocation in multiple sclerosis, Clin. Immunol. 183 (2017) 213–224, https://doi.org/10.1016/j.clim.2017.03.001.

[16] B. Teixeira, V.C.B. Bittencourt, T.B. Ferreira, T.M. Kasahara, P.O. Barros, R. Alvarenga, J. Hygino, R.M. Andrade, A.F. Andrade, C.A.M. Bento, Low sensitivity to glucocorticoid inhibition of in vitro Th17-related cytokine production in multiple sclerosis patients is related to elevated plasma lipopolysaccharide levels, Clin. Immunol. 148 (2013) 209–218, https://doi.org/10.1016/j.clim.2013.05.012.

[17] B. Simbrunner, E. Caparrós, T. Neuwirth, P. Schwabl, P. Königshofer, D. Bauer, R. Marculescu, M. Trauner, B. Scheiner, G. Stary, M. Mandorfer, T. Reiberger, R. Francés, Bacterial translocation occurs early in cirrhosis and triggers a selective inflammatory response, Hepatol Int 17 (2023) 1045–1056, https://doi.org/10.1007/s12072-023-10496-y.

[18] S. Manfredo Vieira, M. Hiltensperger, V. Kumar, D. Zegarra-Ruiz, C. Dehner, N. Khan, F.R.C. Costa, E. Tiniakou, T. Greiling, W. Ruff, A. Barbieri, C. Kriegel, S. S. Mehta, J.R. Knight, D. Jain, A.L. Goodman, M.A. Kriegel, Translocation of a gut pathobiont drives autoimmunity in mice and humans, Science 359 (2018) 1156–1161, https://doi.org/10.1126/science.aar7201.

[19] C. Sorini, I. Cosorich, M. Lo Conte, L. De Giorgi, F. Facciotti, R. Lucianò, M. Rocchi, R. Ferrarese, F. Sanvito, F. Canducci, M. Falcone, Loss of gut barrier integrity triggers activation of islet-reactive T cells and autoimmune diabetes, Proc. Natl. Acad. Sci. U. S. A. 116 (2019) 15140–15149, https://doi.org/10.1073/pnas.1814558116.

[20] M. Kosmidou, A.H. Katsanos, K.H. Katsanos, A.P. Kyritsis, G. Tsivgoulis, D. Christodoulou, S. Giannopoulos, Multiple sclerosis and inflammatory bowel diseases: a systematic review and meta-analysis, J. Neurol. 264 (2017) 254–259, https://doi.org/10.1007/s00415-016-8340-8.

[21] D.J. Levinthal, A. Rahman, S. Nusrat, M. O'Leary, R. Heyman, K. Bielefeldt, Adding to the burden: gastrointestinal symptoms and syndromes in multiple sclerosis, Multiple Sclerosis International 2013 (2013) 1–9, https://doi.org/10.1155/2013/319201.

[22] M.N. Almeida, C. Silvernale, B. Kuo, K. Staller, Bowel symptoms predate the diagnosis among many patients with multiple sclerosis: a 14-year cohort study, Neurogastroenterology Motil 31 (2019) e13592, https://doi.org/10.1111/nmo.13592.

[23] D. Noto, S. Miyake, Gut dysbiosis and multiple sclerosis, Clin. Immunol. 235 (2022) 108380, https://doi.org/10.1016/j.clim.2020.108380.

[24] B.L. Cantarel, E. Waubant, C. Chehoud, J. Kuczynski, T.Z. DeSantis, J. Warrington, A. Venkatesan, C.M. Fraser, E.M. Mowry, Gut microbiota in multiple sclerosis: possible influence of immunomodulators, J. Invest. Med. 63 (2015) 729–734, https://doi.org/10.1097/JIM.0000000000000192.

[25] J. Chen, N. Chia, K.R. Kalari, J.Z. Yao, M. Novotna, M.M. Paz Soldan, D. H. Luckey, E.V. Marietta, P.R. Jeraldo, X. Chen, B.G. Weinshenker, M. Rodriguez, O.H. Kantarci, H. Nelson, J.A. Murray, A.K. Mangalam, Multiple sclerosis patients have a distinct gut microbiota compared to healthy controls, Sci. Rep. 6 (2016) 28484, https://doi.org/10.1038/srep28484.

[26] M. Kozhieva, N. Naumova, T. Alikina, A. Boyko, V. Vlassov, M.R. Kabilov, Primary progressive multiple sclerosis in a Russian cohort: relationship with gut bacterial diversity, BMC Microbiol. 19 (2019) 309, https://doi.org/10.1186/s12866-019-1685-2.

[27] E. Cekanaviciute, B.B. Yoo, T.F. Runia, J.W. Debelius, S. Singh, C.A. Nelson, R. Kanner, Y. Bencosme, Y.K. Lee, S.L. Hauser, E. Crabtree-Hartman, I.K. Sand, M. Gacias, Y. Zhu, P. Casaccia, B.A.C. Cree, R. Knight, S.K. Mazmanian, S. E. Baranzini, Gut bacteria from multiple sclerosis patients modulate human T cells and exacerbate symptoms in mouse models, Proc. Natl. Acad. Sci. U.S.A. 114 (2017) 10713–10718, https://doi.org/10.1073/pnas.1711235114.

[28] A.-C. Paraschiv, V. Vacaras, C. Nistor, C. Vacaras, S. Strilciuc, D.F. Muresanu, The effect of multiple sclerosis therapy on gut microbiota dysbiosis: a longitudinal prospective study, Microb Cell 11 (2024) 106–115, https://doi.org/10.15698/mic2024.03.819.

[29] S. Miyake, S. Kim, W. Suda, K. Oshima, M. Nakamura, T. Matsuoka, N. Chihara, A. Tomita, W. Sato, S.-W. Kim, H. Morita, M. Hattori, T. Yamamura, Dysbiosis in the gut microbiota of patients with multiple sclerosis, with a striking depletion of species belonging to clostridia XIVa and IV clusters, PLoS One 10 (2015) e0137429, https://doi.org/10.1371/journal.pone.0137429.

[30] S.N. Choileáin, M. Kleinewietfeld, K. Raddassi, D.A. Hafler, W.E. Ruff, E. E. Longbrake, CXCR3+ T cells in multiple sclerosis correlate with reduced diversity of the gut microbiome, Journal of Translational Autoimmunity 3 (2020) 100032, https://doi.org/10.1016/j.jtauto.2019.100032.

[31] X. Zhou, R. Baumann, X. Gao, M. Mendoza, S. Singh, I. Katz Sand, Z. Xia, L. M. Cox, T. Chitnis, H. Yoon, L. Moles, S.J. Caillier, A. Santaniello, G. Ackermann, A. Harroud, R. Lincoln, R. Gomez, A. González Peña, E. Digga, D.J. Hakim, Y. Vazquez-Baeza, K. Soman, S. Warto, G. Humphrey, M. Farez, L.A. Gerdes, J. R. Oksenberg, S.S. Zamvil, S. Chandran, P. Connick, D. Otaegui, T. Castillo-Triviño, S.L. Hauser, J.M. Gelfand, H.L. Weiner, R. Hohlfeld, H. Wekerle, J. Graves, A. Bar-Or, B.A.C. Cree, J. Correale, R. Knight, S.E. Baranzini, Gut microbiome of multiple sclerosis patients and paired household healthy controls reveal associations with disease risk and course, Cell 185 (2022) 3467–3486.e16, https://doi.org/10.1016/j.cell.2022.08.021.

[32] A.M. Moser, W. Spindelboeck, H. Strohmaier, C. Enzinger, T. Gattringer, S. Fuchs, F. Fazekas, G. Gorkiewicz, P. Wurm, C. Högenauer, M. Khalil, Mucosal biopsy shows immunologic changes of the colon in patients with early MS, Neurol Neuroimmunol Neuroinflamm 4 (2017) e362, https://doi.org/10.1212/NXI.0000000000000362.

[33] M.C. Buscarinu, S. Romano, R. Mechelli, R. Pizzolato Umeton, M. Ferraldeschi, A. Fornasiero, R. Reniè, B. Cerasoli, E. Morena, C. Romano, N.D. Loizzo, R. Umeton, M. Salvetti, G. Ristori, Intestinal permeability in relapsing-remitting multiple sclerosis, Neurotherapeutics 15 (2018) 68–74, https://doi.org/10.1007/s13311-017-0582-3.

[34] B. Parodi, N. Kerlero De Rosbo, The gut-brain Axis in multiple sclerosis. Is its dysfunction a pathological trigger or a consequence of the disease? Front. Immunol. 12 (2021) 718220 https://doi.org/10.3389/fimmu.2021.718220.

[35] D. Duc, S. Vigne, J. Bernier-Latmani, Y. Yersin, F. Ruiz, N. Gaïa, S. Leo, V. Lazarevic, J. Schrenzel, T.V. Petrova, C. Pot, Disrupting myelin-specific Th17

cell gut homing confers protection in an adoptive transfer experimental autoimmune encephalomyelitis, Cell Rep. 29 (2019) 378–390.e4, https://doi.org/10.1016/j.celrep.2019.09.002.
[36] M. Nouri, A. Bredberg, B. Weström, S. Lavasani, Intestinal barrier dysfunction develops at the onset of experimental autoimmune encephalomyelitis, and can Be induced by adoptive transfer of auto-reactive T cells, PLoS One 9 (2014) e106335, https://doi.org/10.1371/journal.pone.0106335.
[37] D.M. Johanson, J.E. Goertz, I.A. Marin, J. Costello, C.C. Overall, A. Gaultier, Experimental autoimmune encephalomyelitis is associated with changes of the microbiota composition in the gastrointestinal tract, Sci. Rep. 10 (2020) 15183, https://doi.org/10.1038/s41598-020-72197-y.
[38] F. Palermo, N. Pieroni, A. Sanna, B. Parodi, C. Venturi, G. Begani Provinciali, L. Massimi, L. Maugeri, G.P. Marra, E. Longo, L. D'Amico, G. Saccomano, J. Perrin, G. Tromba, I. Bukreeva, M. Fratini, G. Gigli, N. Kerlero De Rosbo, A. Cedola, Multilevel X-ray imaging approach to assess the sequential evolution of multi-organ damage in multiple sclerosis, Commun. Phys. 5 (2022) 290, https://doi.org/10.1038/s42005-022-01070-3.
[39] M. Saresella, I. Marventano, M. Barone, F. La Rosa, F. Piancone, L. Mendozzi, A. d'Arma, V. Rossi, L. Pugnetti, G. Roda, E. Casagni, M.D. Cas, R. Paroni, P. Brigidi, S. Turroni, M. Clerici, Alterations in circulating fatty acid are associated with gut microbiota dysbiosis and inflammation in multiple sclerosis, Front. Immunol. 11 (2020) 1390, https://doi.org/10.3389/fimmu.2020.01390.
[40] I. Spadoni, E. Zagato, A. Bertocchi, R. Paolinelli, E. Hot, A. Di Sabatino, F. Caprioli, L. Bottiglieri, A. Oldani, G. Viale, G. Penna, E. Dejana, M. Rescigno, A gut-vascular barrier controls the systemic dissemination of bacteria, Science 350 (2015) 830–834, https://doi.org/10.1126/science.aad0135.
[41] A.A. Scalise, N. Kakogiannos, F. Zanardi, F. Iannelli, M. Giannotta, The blood–brain and gut–vascular barriers: from the perspective of claudins, Tissue Barriers 9 (2021) 1926190, https://doi.org/10.1080/21688370.2021.1926190.
[42] L. Denzer, W. Muranyi, H. Schroten, C. Schwerk, The role of PLVAP in endothelial cells, Cell Tissue Res. 392 (2023) 393–412, https://doi.org/10.1007/s00441-023-03741-1.
[43] I. Spadoni, A. Pietrelli, G. Pesole, M. Rescigno, Gene expression profile of endothelial cells during perturbation of the gut vascular barrier, Gut Microb. 7 (2016) 540–548, https://doi.org/10.1080/19490976.2016.1239681.
[44] S. Danese, C. Fiocchi, Endothelial cell-immune cell interaction in IBD, Dig. Dis. 34 (2016) 43–50, https://doi.org/10.1159/000442925.
[45] C. Alkim, H. Alkim, A.R. Koksal, S. Boga, I. Sen, Angiogenesis in inflammatory bowel disease, Int. J. Inflamm. 2015 (2015) 1–10, https://doi.org/10.1155/2015/970890.
[46] C. Zhang, H. Chen, Q. He, Y. Luo, A. He, A. Tao, J. Yan, Fibrinogen/AKT/Microfilament Axis promotes colitis by enhancing vascular permeability, Cellular and Molecular Gastroenterology and Hepatology 11 (2021) 683–696, https://doi.org/10.1016/j.jcmgh.2020.10.007.
[47] B. Sun, J. Yuan, S. Wang, J. Lin, W. Zhang, J. Shao, R. Wang, B. Shi, H. Hu, Qingchang suppository ameliorates colonic vascular permeability in dextran-sulfate-sodium-induced colitis, Front. Pharmacol. 9 (2018) 1235, https://doi.org/10.3389/fphar.2018.01235.
[48] J.H. Chidlow, D. Shukla, M.B. Grisham, C.G. Kevil, Pathogenic angiogenesis in IBD and experimental colitis: new ideas and therapeutic avenues, Am. J. Physiol. Gastrointest. Liver Physiol. 293 (2007) G5–G18, https://doi.org/10.1152/ajpgi.00107.2007.
[49] S. Carloni, A. Bertocchi, S. Mancinelli, M. Bellini, M. Erreni, A. Borreca, D. Braga, S. Giugliano, A.M. Mozzarelli, D. Manganaro, D. Fernandez Perez, F. Colombo, A. Di Sabatino, D. Pasini, G. Penna, M. Matteoli, S. Lodato, M. Rescigno, Identification of a choroid plexus vascular barrier closing during intestinal inflammation, Science 374 (2021) 439–448, https://doi.org/10.1126/science.abc6108.
[50] J. Bernier-Latmani, T.V. Petrova, High-resolution 3D analysis of mouse small-intestinal stroma, Nat. Protoc. 11 (2016) 1617–1629, https://doi.org/10.1038/nprot.2016.092.
[51] E. Zudaire, L. Gambardella, C. Kurcz, S. Vermeren, A computational tool for quantitative analysis of vascular networks, PLoS One 6 (2011) e27385, https://doi.org/10.1371/journal.pone.0027385.
[52] J. Huang, C.P. Kelly, K. Bakirtzi, J.A. Villafuerte Gálvez, D. Lyras, S.J. Mileto, S. Larcombe, H. Xu, X. Yang, K.S. Shields, W. Zhu, Y. Zhang, J.D. Goldsmith, I. J. Patel, J. Hansen, M. Huang, S. Yla-Herttuala, A.C. Moss, D. Paredes-Sabja, C. Pothoulakis, Y.M. Shah, J. Wang, X. Chen, Clostridium difficile toxins induce VEGF-A and vascular permeability to promote disease pathogenesis, Nat Microbiol 4 (2018) 269–279, https://doi.org/10.1038/s41564-018-0300-x.
[53] M. Baker, S.D. Robinson, T. Lechertier, P.R. Barber, B. Tavora, G. D'Amico, D. T. Jones, B. Vojnovic, K. Hodivala-Dilke, Use of the mouse aortic ring assay to study angiogenesis, Nat. Protoc. 7 (2012) 89–104, https://doi.org/10.1038/nprot.2011.435.
[54] F. Iqbal, Y.S. Gratch, P. Szaraz, C.L. Librach, The aortic ring Co-culture assay: a convenient tool to assess the angiogenic potential of mesenchymal stromal cells in vitro, JoVE (2017) 56083, https://doi.org/10.3791/56083.
[55] J. Uchida, Y. Hamaguchi, J.A. Oliver, J.V. Ravetch, J.C. Poe, K.M. Haas, T. F. Tedder, The innate mononuclear phagocyte network depletes B lymphocytes through fc receptor–dependent mechanisms during anti-CD20 antibody immunotherapy, J. Exp. Med. 199 (2004) 1659–1669, https://doi.org/10.1084/jem.20040119.
[56] A. Subramanian, P. Tamayo, V.K. Mootha, S. Mukherjee, B.L. Ebert, M.A. Gillette, A. Paulovich, S.L. Pomeroy, T.R. Golub, E.S. Lander, J.P. Mesirov, Gene set enrichment analysis: a knowledge-based approach for interpreting genome-wide expression profiles, Proc. Natl. Acad. Sci. U.S.A. 102 (2005) 15545–15550, https://doi.org/10.1073/pnas.0506580102.
[57] V.K. Mootha, C.M. Lindgren, K.-F. Eriksson, A. Subramanian, S. Sihag, J. Lehar, P. Puigserver, E. Carlsson, M. Ridderstråle, E. Laurila, N. Houstis, M.J. Daly, N. Patterson, J.P. Mesirov, T.R. Golub, P. Tamayo, B. Spiegelman, E.S. Lander, J. N. Hirschhorn, D. Altshuler, L.C. Groop, PGC-1α-responsive genes involved in oxidative phosphorylation are coordinately downregulated in human diabetes, Nat. Genet. 34 (2003) 267–273, https://doi.org/10.1038/ng1180.
[58] A. Liberzon, C. Birger, H. Thorvaldsdóttir, M. Ghandi, J.P. Mesirov, P. Tamayo, The molecular signatures Database hallmark gene set collection, Cell Systems 1 (2015) 417–425, https://doi.org/10.1016/j.cels.2015.12.004.
[59] M. Martin, Cutadapt removes adapter sequences from high-throughput sequencing reads, EMBnet j. 17 (2011) 10, https://doi.org/10.14806/ej.17.1.200.
[60] M.P.A. Davis, S. Van Dongen, C. Abreu-Goodger, N. Bartonicek, A.J. Enright, Kraken: a set of tools for quality control and analysis of high-throughput sequence data, Methods 63 (2013) 41–49, https://doi.org/10.1016/j.ymeth.2013.06.027.
[61] A. Dobin, C.A. Davis, F. Schlesinger, J. Drenkow, C. Zaleski, S. Jha, P. Batut, M. Chaisson, T.R. Gingeras, STAR: ultrafast universal RNA-seq aligner, Bioinformatics 29 (2013) 15–21, https://doi.org/10.1093/bioinformatics/bts635.
[62] S. Anders, P.T. Pyl, W. Huber, HTSeq—a Python framework to work with high-throughput sequencing data, Bioinformatics 31 (2015) 166–169, https://doi.org/10.1093/bioinformatics/btu638.
[63] L. Wang, S. Wang, W. Li, RSeQC: quality control of RNA-seq experiments, Bioinformatics 28 (2012) 2184–2185, https://doi.org/10.1093/bioinformatics/bts356.
[64] M.D. Robinson, D.J. McCarthy, G.K. Smyth, edgeR : a Bioconductor package for differential expression analysis of digital gene expression data, Bioinformatics 26 (2010) 139–140, https://doi.org/10.1093/bioinformatics/btp616.
[65] M.E. Ritchie, B. Phipson, D. Wu, Y. Hu, C.W. Law, W. Shi, G.K. Smyth, Limma powers differential expression analyses for RNA-sequencing and microarray studies, e47–e47, Nucleic Acids Res. 43 (2015), https://doi.org/10.1093/nar/gkv007.
[66] C.S. Abhinand, R. Raju, S.J. Soumya, P.S. Arya, P.R. Sudhakaran, VEGF-A/VEGFR2 signaling network in endothelial cells relevant to angiogenesis, J. Cell Commun. Signal. 10 (2016) 347–354, https://doi.org/10.1007/s12079-016-0352-8.
[67] P. Bianchimano, K. Iwanowski, E.M. Smith, A. Cantor, P. Leone, G. Bongers, C. G. Gonzalez, Y. Hongsup, J. Elias, H.L. Weiner, J.C. Clemente, S.K. Tankou, Oral vancomycin treatment suppresses gut trypsin activity and preserves intestinal barrier function during EAE, iScience 26 (2023) 108143, https://doi.org/10.1016/j.isci.2023.108143.
[68] A. Pettersson, J.A. Nagy, L.F. Brown, C. Sundberg, E. Morgan, S. Jungles, R. Carter, J.E. Krieger, E.J. Manseau, V.S. Harvey, I.A. Eckelhoefer, D. Feng, A. M. Dvorak, R.C. Mulligan, H.F. Dvorak, Heterogeneity of the angiogenic response induced in different normal adult tissues by vascular permeability factor/vascular endothelial growth factor, Lab. Invest. 80 (2000) 99–115, https://doi.org/10.1038/labinvest.3780013.
[69] J.A. Nagy, H.F. Dvorak, Heterogeneity of the tumor vasculature: the need for new tumor blood vessel type-specific targets, Clin. Exp. Metastasis 29 (2012) 657–662, https://doi.org/10.1007/s10585-012-9500-6.
[70] C. Park-Windhol, P.A. D'Amore, Disorders of vascular permeability, Annu. Rev. Pathol. Mech. Dis. 11 (2016) 251–281, https://doi.org/10.1146/annurev-pathol-012615-044506.
[71] G. Thurston, T.J. Murphy, P. Baluk, J.R. Lindsey, D.M. McDonald, Angiogenesis in mice with chronic airway inflammation, Am. J. Pathol. 153 (1998) 1099–1112, https://doi.org/10.1016/S0002-9440(10)65654-4.
[72] F. Lebrin, M.-J. Goumans, L. Jonker, R.L.C. Carvalho, G. Valdimarsdottir, M. Thorikay, C. Mummery, H.M. Arthur, P.T. Dijke, Endoglin promotes endothelial cell proliferation and TGF-β/ALK1 signal transduction, EMBO J. 23 (2004) 4018–4028, https://doi.org/10.1038/sj.emboj.7600386.
[73] G.G. Yegutkin, K. Auvinen, P. Rantakari, M. Hollmén, M. Karikoski, R. Grénman, K. Elima, S. Jalkanen, M. Salmi, Ecto-5′-nucleotidase/CD73 enhances endothelial barrier function and sprouting in blood but not lymphatic vasculature, Eur. J. Immunol. 45 (2015) 562–573, https://doi.org/10.1002/eji.201444856.
[74] N. Di Tommaso, F. Santopaolo, A. Gasbarrini, F.R. Ponziani, The gut–vascular barrier as a new protagonist in intestinal and extraintestinal diseases, IJMS 24 (2023) 1470, https://doi.org/10.3390/ijms24021470.
[75] L. Guo, H. Zhang, Y. Hou, T. Wei, J. Liu, Plasmalemma vesicle-associated protein: a crucial component of vascular homeostasis, Exp. Ther. Med. 12 (2016) 1639–1644, https://doi.org/10.3892/etm.2016.3557.
[76] R.-V. Stan, M. Kubitza, G.E. Palade, PV-1 is a component of the fenestral and stomatal diaphragms in fenestrated endothelia, Proc. Natl. Acad. Sci. U.S.A. 96 (1999) 13203–13207, https://doi.org/10.1073/pnas.96.23.13203.
[77] Y. Wang, H. Yu, X. Xie, T. Deng, L. Ye, L. Wu, X. Ding, Z. Yang, Q. Zhu, J. Li, Y. Zheng, Z. Yu, G. Chen, Plasmalemma vesicle-associated protein promotes angiogenesis in cholangiocarcinoma via the DKK1/CKAP4/PI3K signaling pathway, Oncogene 40 (2021) 4324–4337, https://doi.org/10.1038/s41388-021-01844-z.
[78] J. Keuschnigg, T. Henttinen, K. Auvinen, M. Karikoski, M. Salmi, S. Jalkanen, The prototype endothelial marker PAL-E is a leukocyte trafficking molecule, Blood 114 (2009) 478–484, https://doi.org/10.1182/blood-2008-11-188763.
[79] M. Radu, J. Chernoff, An in vivo assay to test blood vessel permeability, JoVE (2013) 50062, https://doi.org/10.3791/50062.

[80] J. Bernier-Latmani, A. González-Loyola, T.V. Petrova, Mechanisms and functions of intestinal vascular specialization, J. Exp. Med. 221 (2024) e20222008, https://doi.org/10.1084/jem.20222008.

[81] T.Q. Kieu, K. Tazawa, N. Kawashima, S. Noda, M. Fujii, K. Nara, K. Hashimoto, P. Han, T. Okiji, Kinetics of LYVE-1-positive M2-like macrophages in developing and repairing dental pulp in vivo and their pro-angiogenic activity in vitro, Sci. Rep. 12 (2022) 5176, https://doi.org/10.1038/s41598-022-08987-3.

[82] J.W. Opzoomer, J.E. Anstee, I. Dean, E.J. Hill, I. Bouybayoune, J. Caron, T. Muliaditan, P. Gordon, D. Sosnowska, R. Nuamah, S.E. Pinder, T. Ng, F. Dazzi, S. Kordasti, D.R. Withers, T. Lawrence, J.N. Arnold, Macrophages orchestrate the expansion of a proangiogenic perivascular niche during cancer progression, Sci. Adv. 7 (2021) eabg9518, https://doi.org/10.1126/sciadv.abg9518.

[83] C.-H. Cho, Y. Jun Koh, J. Han, H.-K. Sung, H. Jong Lee, T. Morisada, R. A. Schwendener, R.A. Brekken, G. Kang, Y. Oike, T.-S. Choi, T. Suda, O.-J. Yoo, G. Y. Koh, Angiogenic role of LYVE-1–positive macrophages in adipose tissue, Circ. Res. 100 (2007), https://doi.org/10.1161/01.RES.0000259564.92792.93.

[84] G. Gerganova, A. Riddell, A.A. Miller, CNS border-associated macrophages in the homeostatic and ischaemic brain, Pharmacology & Therapeutics 240 (2022) 108220, https://doi.org/10.1016/j.pharmthera.2022.108220.

[85] M.J.C. Jordão, R. Sankowski, S.M. Brendecke, Sagar, G. Locatelli, Y.-H. Tai, T. L. Tay, E. Schramm, S. Armbruster, N. Hagemeyer, O. Groß, D. Mai, Ö. Çiçek, T. Falk, M. Kerschensteiner, D. Grün, M. Prinz, Single-cell profiling identifies myeloid cell subsets with distinct fates during neuroinflammation, Science 363 (2019), https://doi.org/10.1126/science.aat7554 eaat7554.

[86] P. Chiaranunt, K. Burrows, L. Ngai, S.L. Tai, E.Y. Cao, H. Liang, H. Hamidzada, A. Wong, J. Gschwend, P. Flüchter, M. Kuypers, T. Despot, A. Momen, S.M. Lim, T. Mallevaey, C. Schneider, T. Conway, H. Imamura, S. Epelman, A. Mortha, Microbial energy metabolism fuels an intestinal macrophage niche in solitary isolated lymphoid tissues through purinergic signaling, Sci. Immunol. 8 (2023) eabq4573, https://doi.org/10.1126/sciimmunol.abq4573.

[87] A.-K. Pröbstel, X. Zhou, R. Baumann, S. Wischnewski, M. Kutza, O.L. Rojas, K. Sellrie, A. Bischof, K. Kim, A. Ramesh, R. Dandekar, A.L. Greenfield, R. D. Schubert, J.E. Bisanz, S. Vistnes, K. Khaleghi, J. Landefeld, G. Kirkish, F. Liesche-Starnecker, V. Ramaglia, S. Singh, E.B. Tran, P. Barba, K. Zorn, J. Oechtering, K. Forsberg, L.R. Shiow, R.G. Henry, J. Graves, B.A.C. Cree, S. L. Hauser, J. Kuhle, J.M. Gelfand, P.M. Andersen, J. Schlegel, P.J. Turnbaugh, P. H. Seeberger, J.L. Gommerman, M.R. Wilson, L. Schirmer, S.E. Baranzini, Gut microbiota–specific IgA $^{+}$ B cells traffic to the CNS in active multiple sclerosis, Sci. Immunol. 5 (2020), https://doi.org/10.1126/sciimmunol.abc7191 eabc7191.

[88] O.L. Rojas, A.-K. Pröbstel, E.A. Porfilio, A.A. Wang, M. Charabati, T. Sun, D.S. W. Lee, G. Galicia, V. Ramaglia, L.A. Ward, L.Y.T. Leung, G. Najafi, K. Khaleghi, B. Garcillán, A. Li, R. Besla, I. Naouar, E.Y. Cao, P. Chiaranunt, K. Burrows, H. G. Robinson, J.R. Allanach, J. Yam, H. Luck, D.J. Campbell, D. Allman, D. G. Brooks, M. Tomura, R. Baumann, S.S. Zamvil, A. Bar-Or, M.S. Horwitz, D. A. Winer, A. Mortha, F. Mackay, A. Prat, L.C. Osborne, C. Robbins, S.E. Baranzini, J.L. Gommerman, Recirculating intestinal IgA-producing cells regulate neuroinflammation via IL-10, Cell 176 (2019) 610–624.e18, https://doi.org/10.1016/j.cell.2018.11.035.

[89] C. Tsui, N. Martinez-Martin, M. Gaya, P. Maldonado, M. Llorian, N.M. Legrave, M. Rossi, J.I. MacRae, A.J. Cameron, P.J. Parker, M. Leitges, A. Bruckbauer, F. D. Batista, Protein kinase C-β dictates B cell fate by regulating mitochondrial remodeling, metabolic reprogramming, and heme biosynthesis, Immunity 48 (2018) 1144–1159.e5, https://doi.org/10.1016/j.immuni.2018.04.031.

[90] J. Kunisawa, Y. Sugiura, T. Wake, T. Nagatake, H. Suzuki, R. Nagasawa, S. Shikata, K. Honda, E. Hashimoto, Y. Suzuki, M. Setou, M. Suematsu, H. Kiyono, Mode of bioenergetic metabolism during B cell differentiation in the intestine determines the distinct requirement for vitamin B1, Cell Rep. 13 (2015) 122–131, https://doi.org/10.1016/j.celrep.2015.08.063.

[91] M.J. Price, D.G. Patterson, C.D. Scharer, J.M. Boss, Progressive upregulation of oxidative metabolism facilitates plasmablast differentiation to a T-independent antigen, Cell Rep. 23 (2018) 3152–3159, https://doi.org/10.1016/j.celrep.2018.05.053.

[92] J. Kunisawa, Metabolic changes during B cell differentiation for the production of intestinal IgA antibody, Cell. Mol. Life Sci. 74 (2017) 1503–1509, https://doi.org/10.1007/s00018-016-2414-8.

[93] X. Sun, P.D. Kaufman, Ki-67: more than a proliferation marker, Chromosoma 127 (2018) 175–186, https://doi.org/10.1007/s00412-018-0659-8.

[94] J. Yuan, R. Yan, A. Krämer, F. Eckerdt, M. Roller, M. Kaufmann, K. Strebhardt, Cyclin B1 depletion inhibits proliferation and induces apoptosis in human tumor cells, Oncogene 23 (2004) 5843–5852, https://doi.org/10.1038/sj.onc.1207757.

[95] N.W. Kam, K.C. Wu, W. Dai, Y. Wang, L.Y.C. Yan, R. Shakya, R. Khanna, Y. Qin, S. Law, A.W.I. Lo, V.H.F. Lee, X.-Y. Guan, D.L.-W. Kwong, Peritumoral B cells drive proangiogenic responses in HMGB1-enriched esophageal squamous cell carcinoma, Angiogenesis 25 (2022) 181–203, https://doi.org/10.1007/s10456-021-09819-0.

[96] W. Van De Veen, A. Globinska, K. Jansen, A. Straumann, T. Kubo, D. Verschoor, O.F. Wirz, F. Castro-Giner, G. Tan, B. Rückert, U. Ochsner, M. Herrmann, B. Stanić, M. Van Splunter, D. Huntjens, A. Wallimann, R.J. Fonseca Guevara, H. Spits, D. Ignatova, Y.-T. Chang, C. Fassnacht, E. Guenova, L. Flatz, C.A. Akdis, M. Akdis, A novel proangiogenic B cell subset is increased in cancer and chronic inflammation, Sci. Adv. 6 (2020) eaaz3559, https://doi.org/10.1126/sciadv.aaz3559.

[97] N. Bach, R. Winzer, E. Tolosa, W. Fiedler, F. Brauneck, The clinical significance of CD73 in cancer, IJMS 24 (2023) 11759, https://doi.org/10.3390/ijms241411759.

[98] G. Ghalamfarsa, A. Rastegari, F. Atyabi, H. Hassannia, M. Hojjat-Farsangi, A. Ghanbari, E. Anvari, J. Mohammadi, G. Azizi, A. Masjedi, M. Yousefi, B. Yousefi, J. Hadjati, F. Jadidi-Niaragh, Anti-angiogenic effects of CD73-specific siRNA-loaded nanoparticles in breast cancer-bearing mice, J. Cell. Physiol. 233 (2018) 7165–7177, https://doi.org/10.1002/jcp.26743.

[99] P. Koszałka, A. Pryszlak, M. Gołuńska, J. Kolasa, G. Stasiłojć, A.C. Składanowski, J.J. Bigda, Inhibition of CD73 stimulates the migration and invasion of B16F10 melanoma cells in vitro, but results in impaired angiogenesis and reduced melanoma growth in vivo, Oncol. Rep. 31 (2014) 819–827, https://doi.org/10.3892/or.2013.2883.

[100] N.M. Weisel, S.M. Joachim, S. Smita, D. Callahan, R.A. Elsner, L.J. Conter, M. Chikina, D.L. Farber, F.J. Weisel, M.J. Shlomchik, Surface phenotypes of naive and memory B cells in mouse and human tissues, Nat. Immunol. 23 (2022) 135–145, https://doi.org/10.1038/s41590-021-01078-x.

[101] A. Szade, A. Grochot-Przeczek, U. Florczyk, A. Jozkowicz, J. Dulak, Cellular and molecular mechanisms of inflammation-induced angiogenesis, IUBMB Life 67 (2015) 145–159, https://doi.org/10.1002/iub.1358.

[102] G.J. Hoilat, A.K. Altowairqi, M.F. Ayas, N.T. Alhaddab, R.A. Alnujaidi, H. A. Alharbi, N. Alyahyawi, A. Kamal, H. Alhabeeb, E. Albazee, S. Almustanyir, A. Abu-Zaid, Larazotide acetate for treatment of celiac disease: a systematic review and meta-analysis of randomized controlled trials, Clinics and Research in Hepatology and Gastroenterology 46 (2022) 101782, https://doi.org/10.1016/j.clinre.2021.101782.

[103] C. Sturgeon, J. Lan, A. Fasano, Zonulin transgenic mice show altered gut permeability and increased morbidity/mortality in the DSS colitis model, Ann. N. Y. Acad. Sci. 1397 (2017) 130–142, https://doi.org/10.1111/nyas.13343.

[104] J. Mouries, P. Brescia, A. Silvestri, I. Spadoni, M. Sorribas, R. Wiest, E. Mileti, M. Galbiati, P. Invernizzi, L. Adorini, G. Penna, M. Rescigno, Microbiota-driven gut vascular barrier disruption is a prerequisite for non-alcoholic steatohepatitis development, J. Hepatol. 71 (2019) 1216–1228, https://doi.org/10.1016/j.jhep.2019.08.005.

[105] A. Bertocchi, S. Carloni, P.S. Ravenda, G. Bertalot, I. Spadoni, A. Lo Cascio, S. Gandini, M. Lizier, D. Braga, F. Asnicar, N. Segata, C. Klaver, P. Brescia, E. Rossi, A. Anselmo, S. Guglietta, A. Maroli, P. Spaggiari, N. Tarazona, A. Cervantes, S. Marsoni, L. Lazzari, M.G. Jodice, C. Luise, M. Erreni, S. Pece, P. P. Di Fiore, G. Viale, A. Spinelli, C. Pozzi, G. Penna, M. Rescigno, Gut vascular barrier impairment leads to intestinal bacteria dissemination and colorectal cancer metastasis to liver, Cancer Cell 39 (2021) 708–724.e11, https://doi.org/10.1016/j.ccell.2021.03.004.

[106] C. Zhang, X. Cao, H. Wang, Z. Li, Y. Zhang, The ACE2 activator diminazene aceturate ameliorates colitis by repairing the gut-vascular barrier in mice, Microvasc. Res. 148 (2023) 104544, https://doi.org/10.1016/j.mvr.2023.104544.

[107] T. Korn, M. Mitsdoerffer, A.L. Croxford, A. Awasthi, V.A. Dardalhon, G. Galileos, P. Vollmar, G.L. Stritesky, M.H. Kaplan, A. Waisman, V.K. Kuchroo, M. Oukka, IL-6 controls Th17 immunity in vivo by inhibiting the conversion of conventional T cells into Foxp3 $^{+}$ regulatory T cells, Proc. Natl. Acad. Sci. U.S.A. 105 (2008) 18460–18465, https://doi.org/10.1073/pnas.0809850105.

[108] B. Hansen, R. Hussain, A. Lovettracke, J. Thomas, M. Racke, Multiple toll-like receptor agonists act as potent adjuvants in the induction of autoimmunity, J. Neuroimmunol. 172 (2006) 94–103, https://doi.org/10.1016/j.jneuroim.2005.11.006.

[109] L. Visser, H. Jan De Heer, L.A. Boven, D. Van Riel, M. Van Meurs, M.-J. Melief, U. Zähringer, J. Van Strijp, B.N. Lambrecht, E.E. Nieuwenhuis, J.D. Laman, Proinflammatory bacterial peptidoglycan as a cofactor for the development of central nervous system autoimmune disease, J. Immunol. 174 (2005) 808–816, https://doi.org/10.4049/jimmunol.174.2.808.

[110] J.A. Fontes, J.G. Barin, M.V. Talor, N. Stickel, J. Schaub, N.R. Rose, D. Čiháková, Complete Freund's adjuvant induces experimental autoimmune myocarditis by enhancing IL-6 production during initiation of the immune response: IL-6 in the initiation of EAM, Immunity, Inflammation and Disease 5 (2017) 163–176, https://doi.org/10.1002/iid3.155.

[111] J.S. Ellis, B.M. Chain, A. Cooke, M.A. Ibrahim, D.R. Katz, Adjuvant composition determines the induction of type II collagen-induced arthritis, Scand. J. Immunol. 36 (1992) 49–56, https://doi.org/10.1111/j.1365-3083.1992.tb02939.x.

[112] D.A. Simpkins, P. Downton, K.J. Gray, S.H. Dickson, R.J. Maidstone, J.E. Konkel, M.R. Hepworth, D.W. Ray, D.A. Bechtold, J.E. Gibbs, Consequences of collagen induced inflammatory arthritis on circadian regulation of the gut microbiome, Faseb. J. 37 (2023), https://doi.org/10.1096/fj.202201728R.

[113] J.G. Barin, M.V. Talor, N.L. Diny, S. Ong, J.A. Schaub, E. Gebremariam, D. Bedja, G. Chen, H.S. Choi, X. Hou, L. Wu, A.B. Cardamone, D.A. Peterson, N.R. Rose, D. Čiháková, Regulation of autoimmune myocarditis by host responses to the microbiome, Exp. Mol. Pathol. 103 (2017) 141–152, https://doi.org/10.1016/j.yexmp.2017.08.003.

[114] E. Kopczyńska, R. Makarewicz, Endoglin – a marker of vascular endothelial cell proliferation in cancer, Wo 1 (2012) 68–71, https://doi.org/10.5114/wo.2012.27340.

[115] S. Lamy, M.-P. Lachambre, S. Lord-Dufour, R. Béliveau, Propranolol suppresses angiogenesis in vitro: inhibition of proliferation, migration, and differentiation of endothelial cells, Vasc. Pharmacol. 53 (2010) 200–208, https://doi.org/10.1016/j.vph.2010.08.002.

[116] C. Ollauri-Ibáñez, J.M. López-Novoa, M. Pericacho, Endoglin-based biological therapy in the treatment of angiogenesis-dependent pathologies, Expet Opin. Biol. Ther. 17 (2017) 1053–1063, https://doi.org/10.1080/14712598.2017.1346607.

[117] S. Karampoor, H. Zahednasab, S. Ramagopalan, M. Mehrpour, H. Keyvani, Angiogenic factors are associated with multiple sclerosis, J. Neuroimmunol. 301 (2016) 88–93, https://doi.org/10.1016/j.jneuroim.2016.11.005.
[118] C.J. MacMillan, S.J. Furlong, C.D. Doucette, P.-L. Chen, D.W. Hoskin, A.S. Easton, Bevacizumab diminishes experimental autoimmune encephalomyelitis by inhibiting spinal cord angiogenesis and reducing peripheral T-cell responses, J. Neuropathol. Exp. Neurol. 71 (2012) 983–999, https://doi.org/10.1097/NEN.0b013e3182724831.
[119] D.O. Bates, Vascular endothelial growth factors and vascular permeability, Cardiovasc. Res. 87 (2010) 262–271, https://doi.org/10.1093/cvr/cvq105.
[120] D.O. Bates, N.J. Hillman, B. Williams, C.R. Neal, T.M. Pocock, Regulation of microvascular permeability by vascular endothelial growth factors, J. Anat. 200 (2002) 581–597, https://doi.org/10.1046/j.1469-7580.2002.00066.x.
[121] M. Nouri, B. Weström, S. Lavasani, Elevated fecal calprotectin accompanied by intestinal neutrophil infiltration and goblet cell hyperplasia in a murine model of multiple sclerosis, IJMS 24 (2023) 15367, https://doi.org/10.3390/ijms242015367.
[122] L. Wang, H. Luo, X. Chen, Y. Jiang, Q. Huang, Functional characterization of S100A8 and S100A9 in altering monolayer permeability of human umbilical endothelial cells, PLoS One 9 (2014) e90472, https://doi.org/10.1371/journal.pone.0090472.
[123] R. Yu, Q. Zhou, T. Liu, P. Liu, H. Li, Y. Bian, Z. Liu, Kaempferol relieves the DSS-induced chronic colitis in C57BL/6J mice, alleviates intestinal angiogenesis, and regulates colonic microflora structure, J. Funct.Foods 107 (2023) 105646, https://doi.org/10.1016/j.jff.2023.105646.
[124] T. Chu, R. Yu, Y. Gu, Y. Wang, H. Chang, Y. Li, J. Li, Y. Bian, Kaempferol protects gut-vascular barrier from high glucose induced disorder via NF-κB pathway, J. Nutr. Biochem. (2023) 109496, https://doi.org/10.1016/j.jnutbio.2023.109496.
[125] S. Banerji, J. Ni, S.-X. Wang, S. Clasper, J. Su, R. Tammi, M. Jones, D.G. Jackson, LYVE-1, a new homologue of the CD44 glycoprotein, is a lymph-specific receptor for hyaluronan, J. Cell Biol. 144 (1999) 789–801, https://doi.org/10.1083/jcb.144.4.789.
[126] C. Mouta Carreira, S.M. Nasser, E. di Tomaso, T.P. Padera, Y. Boucher, S. I. Tomarev, R.K. Jain, LYVE-1 is not restricted to the lymph vessels: expression in normal liver blood sinusoids and down-regulation in human liver cancer and cirrhosis, Cancer Res. 61 (2001) 8079–8084.
[127] M. Zheng, S. Kimura, J. Nio-Kobayashi, T. Iwanaga, The selective distribution of LYVE-1-expressing endothelial cells and reticular cells in the reticulo-endothelial system (RES), Biomed Res 37 (2016) 187–198, https://doi.org/10.2220/biomedres.37.187.
[128] R. Prevo, S. Banerji, D.J.P. Ferguson, S. Clasper, D.G. Jackson, Mouse LYVE-1 is an endocytic receptor for hyaluronan in lymphatic endothelium, J. Biol. Chem. 276 (2001) 19420–19430, https://doi.org/10.1074/jbc.M011004200.
[129] L.A. Johnson, S. Banerji, W. Lawrance, U. Gileadi, G. Prota, K.A. Holder, Y. M. Roshorm, T. Hanke, V. Cerundolo, N.W. Gale, D.G. Jackson, Dendritic cells enter lymph vessels by hyaluronan-mediated docking to the endothelial receptor LYVE-1, Nat. Immunol. 18 (2017) 762–770, https://doi.org/10.1038/ni.3750.
[130] M.E. Mummert, D. Mummert, D. Edelbaum, F. Hui, H. Matsue, A. Takashima, Synthesis and surface expression of hyaluronan by dendritic cells and its potential role in antigen presentation, J. Immunol. 169 (2002) 4322–4331, https://doi.org/10.4049/jimmunol.169.8.4322.
[131] N.N. Lynskey, S. Banerji, L.A. Johnson, K.A. Holder, M. Reglinski, P.A.C. Wing, D. Rigby, D.G. Jackson, S. Sriskandan, Rapid lymphatic dissemination of encapsulated group A streptococci via lymphatic vessel endothelial receptor-1 interaction, PLoS Pathog. 11 (2015) e1005137, https://doi.org/10.1371/journal.ppat.1005137.
[132] S.E. Armstrong, D.R. Bell, Measurement of high-molecular-weight hyaluronan in solid tissue using agarose gel electrophoresis, Anal. Biochem. 308 (2002) 255–264, https://doi.org/10.1016/s0003-2697(02)00239-7.
[133] C.A. De La Motte, V.C. Hascall, J. Drazba, S.K. Bandyopadhyay, S.A. Strong, Mononuclear leukocytes bind to specific hyaluronan structures on colon mucosal smooth muscle cells treated with polyinosinic acid:polycytidylic acid, Am. J. Pathol. 163 (2003) 121–133, https://doi.org/10.1016/S0002-9440(10)63636-X.
[134] P.M. Bartold, R.C. Page, The effect of chronic inflammation on gingival connective tissue proteoglycans and hyaluronic acid, J. Oral Pathol. Med. 15 (1986) 367–374, https://doi.org/10.1111/j.1600-0714.1986.tb00643.x.
[135] S.M. Casalino-Matsuda, M.E. Monzón, R.M. Forteza, Epidermal growth factor receptor activation by epidermal growth factor mediates oxidant-induced goblet cell metaplasia in human airway epithelium, Am. J. Respir. Cell Mol. Biol. 34 (2006) 581–591, https://doi.org/10.1165/rcmb.2005-0386OC.
[136] P.L. Bollyky, J.D. Lord, S.A. Masewicz, S.P. Evanko, J.H. Buckner, T.N. Wight, G. T. Nepom, Cutting edge: high molecular weight hyaluronan promotes the suppressive effects of CD4+CD25+ regulatory T cells, J. Immunol. 179 (2007) 744–747, https://doi.org/10.4049/jimmunol.179.2.744.
[137] D.C. West, S. Kumar, The effect of hyaluronate and its oligosaccharides on endothelial cell proliferation and monolayer integrity, Exp. Cell Res. 183 (1989) 179–196, https://doi.org/10.1016/0014-4827(89)90428-X.
[138] M. Romo, C. López-Vicario, N. Pérez-Romero, M. Casulleras, A.I. Martínez-Puchol, B. Sánchez, R. Flores-Costa, J. Alcaraz-Quiles, M. Duran-Güell, A. Ibarzábal, J.J. Espert, J. Clària, E. Titos, Small fragments of hyaluronan are increased in individuals with obesity and contribute to low-grade inflammation through TLR-mediated activation of innate immune cells, Int. J. Obes. 46 (2022) 1960–1969, https://doi.org/10.1038/s41366-022-01187-z.
[139] C. Termeer, F. Benedix, J. Sleeman, C. Fieber, U. Voith, T. Ahrens, K. Miyake, M. Freudenberg, C. Galanos, J.C. Simon, Oligosaccharides of hyaluronan activate dendritic cells via toll-like receptor 4, J. Exp. Med. 195 (2002) 99–111, https://doi.org/10.1084/jem.20001858.
[140] Y. Wang, G. Han, B. Guo, J. Huang, Hyaluronan oligosaccharides promote diabetic wound healing by increasing angiogenesis, Pharmacol. Rep. 68 (2016) 1126–1132, https://doi.org/10.1016/j.pharep.2016.07.001.
[141] A. Genasetti, D. Vigetti, M. Viola, E. Karousou, P. Moretto, M. Rizzi, B. Bartolini, M. Clerici, F. Pallotti, G. De Luca, A. Passi, Hyaluronan and human endothelial cell behavior, Connect. Tissue Res. 49 (2008) 120–123, https://doi.org/10.1080/03008200802148462.
[142] D. Jiang, J. Liang, J. Fan, S. Yu, S. Chen, Y. Luo, G.D. Prestwich, M. M. Mascarenhas, H.G. Garg, D.A. Quinn, R.J. Homer, D.R. Goldstein, R. Bucala, P. J. Lee, R. Medzhitov, P.W. Noble, Regulation of lung injury and repair by Toll-like receptors and hyaluronan, Nat. Med. 11 (2005) 1173–1179, https://doi.org/10.1038/nm1315.
[143] T.E. Riehl, X. Ee, W.F. Stenson, Hyaluronic acid regulates normal intestinal and colonic growth in mice, Am. J. Physiol. Gastrointest. Liver Physiol. 303 (2012) G377–G388, https://doi.org/10.1152/ajpgi.00034.2012.
[144] L. Zheng, T.E. Riehl, W.F. Stenson, Regulation of colonic epithelial repair in mice by toll-like receptors and hyaluronic acid, Gastroenterology 137 (2009) 2041–2051, https://doi.org/10.1053/j.gastro.2009.08.055.
[145] A.M. Mueller, B.H. Yoon, S.A. Sadiq, Inhibition of hyaluronan synthesis protects against central nervous system (CNS) autoimmunity and increases CXCL12 expression in the inflamed CNS, J. Biol. Chem. 289 (2014) 22888–22899, https://doi.org/10.1074/jbc.M114.559583.
[146] S.L. Hauser, A. Bar-Or, G. Comi, G. Giovannoni, H.-P. Hartung, B. Hemmer, F. Lublin, X. Montalban, K.W. Rammohan, K. Selmaj, A. Traboulsee, J. S. Wolinsky, D.L. Arnold, G. Klingelschmitt, D. Masterman, P. Fontoura, S. Belachew, P. Chin, N. Mairon, H. Garren, L. Kappos, Ocrelizumab versus interferon beta-1a in relapsing multiple sclerosis, N. Engl. J. Med. 376 (2017) 221–234, https://doi.org/10.1056/NEJMoa1601277.
[147] D.S.W. Lee, O.L. Rojas, J.L. Gommerman, B cell depletion therapies in autoimmune disease: advances and mechanistic insights, Nat. Rev. Drug Discov. 20 (2021) 179–199, https://doi.org/10.1038/s41573-020-00092-2.
[148] H.Y. Lim, S.Y. Lim, C.K. Tan, C.H. Thiam, C.C. Goh, D. Carbajo, S.H.S. Chew, P. See, S. Chakarov, X.N. Wang, L.H. Lim, L.A. Johnson, J. Lum, C.Y. Fong, A. Bongso, A. Biswas, C. Goh, M. Evrard, K.P. Yeo, R. Basu, J.K. Wang, Y. Tan, R. Jain, S. Tikoo, C. Choong, W. Weninger, M. Poidinger, R.E. Stanley, M. Collin, N.S. Tan, L.G. Ng, D.G. Jackson, F. Ginhoux, V. Angeli, Hyaluronan receptor LYVE-1-expressing macrophages maintain arterial tone through hyaluronan-mediated regulation of smooth muscle cell collagen, Immunity 49 (2018) 326–341.e7, https://doi.org/10.1016/j.immuni.2018.06.008.
[149] A. Takeda, M.S. Hossain, P. Rantakari, S. Simmons, N. Sasaki, M. Salmi, S. Jalkanen, M. Miyasaka, Thymocytes in lyve1-CRE/S1pr1f/f mice accumulate in the thymus due to cell-intrinsic loss of sphingosine-1-phosphate receptor expression, Front. Immunol. 7 (2016), https://doi.org/10.3389/fimmu.2016.00489.
[150] A. Rafi, M. Nagarkatti, P.S. Nagarkatti, Hyaluronate-CD44 interactions can induce murine B-cell activation, Blood 89 (1997) 2901–2908.
[151] S. Ghosh, S.A. Hoselton, S.B. Wanjara, J. Carlson, J.B. McCarthy, G.P. Dorsam, J. M. Schuh, Hyaluronan stimulates ex vivo B lymphocyte chemotaxis and cytokine production in a murine model of fungal allergic asthma, Immunobiology 220 (2015) 899–909, https://doi.org/10.1016/j.imbio.2015.01.011.
[152] Y. Iwata, A. Yoshizaki, K. Komura, K. Shimizu, F. Ogawa, T. Hara, E. Muroi, S. Bae, M. Takenaka, T. Yukami, M. Hasegawa, M. Fujimoto, Y. Tomita, T. F. Tedder, S. Sato, CD19, a response regulator of B lymphocytes, regulates wound healing through hyaluronan-induced TLR4 signaling, Am. J. Pathol. 175 (2009) 649–660, https://doi.org/10.2353/ajpath.2009.080355.
[153] D. Vigetti, A. Genasetti, E. Karousou, M. Viola, P. Moretto, M. Clerici, S. Deleonibus, G. De Luca, V.C. Hascall, A. Passi, Proinflammatory cytokines induce hyaluronan synthesis and monocyte adhesion in human endothelial cells through hyaluronan synthase 2 (HAS2) and the nuclear factor-κB (NF-κB) pathway, J. Biol. Chem. 285 (2010) 24639–24645, https://doi.org/10.1074/jbc.M110.134536.
[154] S.P. Colgan, H.K. Eltzschig, T. Eckle, L.F. Thompson, Physiological roles for ecto-5'-nucleotidase (CD73), Purinergic Signal. 2 (2006) 351–360, https://doi.org/10.1007/s11302-005-5302-5.
[155] J.A. Auchampach, Adenosine receptors and angiogenesis, Circ. Res. 101 (2007) 1075–1077, https://doi.org/10.1161/CIRCRESAHA.107.165761.
[156] I. Ernens, M. Bousquenaud, B. Lenoir, Y. Devaux, D.R. Wagner, Adenosine stimulates angiogenesis by up-regulating production of thrombospondin-1 by macrophages, J. Leukoc. Biol. 97 (2015) 9–18, https://doi.org/10.1189/jlb.3HI0514-249RR.
[157] B. Allard, M. Turcotte, K. Spring, S. Pommey, I. Royal, J. Stagg, Anti-CD73 therapy impairs tumor angiogenesis, Intl Journal of Cancer 134 (2014) 1466–1473, https://doi.org/10.1002/ijc.28456.
[158] X. Cao, Z. Zhu, Y. Cao, J. Hu, M. Min, CD73 is a hypoxia-responsive gene and promotes the Warburg effect of human gastric cancer cells dependent on its enzyme activity, J. Cancer 12 (2021) 6372–6382, https://doi.org/10.7150/jca.62387.
[159] H.S. Sperber, K.A. Raymond, M.S. Bouzidi, T. Ma, S. Valdebenito, E.A. Eugenin, N. R. Roan, S.G. Deeks, S. Winning, J. Fandrey, R. Schwarzer, S.K. Pillai, The hypoxia-regulated ectonucleotidase CD73 is a host determinant of HIV latency, Cell Rep. 42 (2023) 113285, https://doi.org/10.1016/j.celrep.2023.113285.
[160] X. Li, T. Zhou, X. Zhi, F. Zhao, L. Yin, P. Zhou, Effect of hypoxia/reoxygenation on CD73 (ecto-5′-nucleotidase) in mouse microvessel endothelial cell lines, Microvasc. Res. 72 (2006) 48–53, https://doi.org/10.1016/j.mvr.2006.04.005.

[161] J.H. Mills, L.F. Thompson, C. Mueller, A.T. Waickman, S. Jalkanen, J. Niemela, L. Airas, M.S. Bynoe, CD73 is required for efficient entry of lymphocytes into the central nervous system during experimental autoimmune encephalomyelitis, Proc. Natl. Acad. Sci. U.S.A. 105 (2008) 9325–9330, https://doi.org/10.1073/pnas.0711175105.

[162] G. Hernandez-Mir, M.J. McGeachy, CD73 is expressed by inflammatory Th17 cells in experimental autoimmune encephalomyelitis but does not limit differentiation or pathogenesis, PLoS One 12 (2017) e0173655, https://doi.org/10.1371/journal.pone.0173655.

[163] J.J. Ahn, Y. Islam, C. Clarkson-Paredes, M.T. Karl, R.H. Miller, B cell depletion modulates glial responses and enhances blood vessel integrity in a model of multiple sclerosis, Neurobiol. Dis. 187 (2023) 106290, https://doi.org/10.1016/j.nbd.2023.106290.

[164] M.S. Bynoe, A.T. Waickman, D.A. Mahamed, C. Mueller, J.H. Mills, A. Czopik, CD73 is critical for the resolution of murine colonic inflammation, J. Biomed. Biotechnol. 2012 (2012) 1–13, https://doi.org/10.1155/2012/260983.